UNIVERSIDADE FEDERAL DE PERNAMBUCO
DEPARTAMENTO DE FÍSICA – CCEN
PROGRAMA DE PÓS-GRADUAÇÃO EM FÍSICA

PAULO CÉSAR DO NASCIMENTO PEREIRA

ENERGY AND INTERACTION FORCES IN CLASSICAL TWO-DIMENSIONAL CRYSTALS WITH INHOMOGENEOUS COARSE-GRAINED DENSITY

Recife
2016

PAULO CÉSAR DO NASCIMENTO PEREIRA

ENERGY AND INTERACTION FORCES IN CLASSICAL TWO-DIMENSIONAL CRYSTALS WITH INHOMOGENEOUS COARSE-GRAINED DENSITY

Dissertação apresentada ao Programa de Pós-Graduação em Física da Universidade Federal de Pernambuco, como requisito parcial para a obtenção do título de Mestre em Física.

Orientador:
Prof. Dr. Sérgio Wlademir da Silva Apolinário
Universidade Federal de Pernambuco

Recife
2016

Catalogação na fonte
Bibliotecária Joana D'Arc Leão Salvador CRB 4-572

P436e Pereira, Paulo César do Nascimento.
Energy and interaction forces in classical two-dimensional crystals with inhomogeneous goarse-grained density / Paulo César do Nascimento Pereira . – 2016.
51 f.: fig.

Orientador: Sérgio Wlademir da Silva Apolinário.
Dissertação (Mestrado) – Universidade Federal de Pernambuco. CCEN. Física. Recife, 2016.
Inclui referências.

1. Matéria condensada. 2. Elasticidade. I. Apolinário, Sérgio Wlademir da Silva (Orientador). II. Titulo.

530.41 CDD (22. ed.) UFPE-FQ 2016-41

PAULO CÉSAR DO NASCIMENTO PEREIRA

ENERGY AND INTERACTION FORCES IN CLASSICAL TWO-DIMENSIONAL CRYSTALS WITH INHOMOGENEOUS COARSE-GRAINED DENSITY

Dissertação apresentada ao Programa de Pós-Graduação em Física da Universidade Federal de Pernambuco, como requisito parcial para a obtenção do título de Mestre em Física.

Aprovada em: 13/04/2016.

BANCA EXAMINADORA

_____
Prof. Dr. Sérgio Wlademir da Silva Apolinário
Orientador
Universidade Federal de Pernambuco

_____
Prof. Dr. Antônio Murilo Santos Macêdo
Examinador Interno
Universidade Federal de Pernambuco

_____
Prof. Dr. Wandemberg Paiva Ferreira
Examinador Externo
Universidade Federal do Ceará

Acknowledgements

I would like to thank many friends, but specially my family, my advisor Sérgio Apolinario, the other members of our laboratory (namely, Lucas Costa Campos, Rafael Jungmann and Everton Lima) and Antônio Murilo Macêdo.

"I am very odd. That is to say, I am methodical, orderly and logical - and I do not like distorting facts to support a theory. That, I find, is unusual!"

—AGATHA CHRISTIE (Hercule Poirot (or Science...) at "One, Two, Buckle My Shoe", 1940)

Abstract

In this M.Sc. thesis, we concentrate on classical two-dimensional crystals with soft pairwise interactions at low temperatures. Typically, the triangular lattice is the configuration which minimizes the interaction potential energy. Such energy is calculated through a lattice sum and we show some analytical approximations to it. We will be interested in cases where the coarse-grained density slightly depends on position. This can be caused by an external force on particles. Then the softness of interactions will determine how the coarse-grained density must vary. At equilibrium, the density gradient generates an equal and opposite force, resultant from interactions. In the limit of small gradients, the system has few defects and locally conserves the triangular lattice symmetry. Although the system's configuration has a huge number of freedom degrees, only the position dependence of coarse-grained density is our relevant information at scales much greater than the nearest-neighbors' distance. We then investigate the calculation of the resultant interaction force due to such density variations with position. A simple and intuitive, but not rigorous, way to obtain the Dynamical Density Functional Theory (DDFT) force is showed. Also, a microscopic approach giving the same result is proposed. In equilibrium, this force gives a minimization of the total free energy and it has been successful in many nonequilibrium systems. We show that this force fails in the case of long wavelength longitudinal waves, giving a smaller result for the sound speed. Also, in recent computer simulations, we obtained equilibrium configurations where the same correction in the force is needed. We show that such correction can be obtained by adding a correction term in the free energy, calculated as a functional of coarse-grained density.

Keywords: Soft Condensed Matter. Two-dimensional Crystals. Dynamical Density Functional Theory. Sound Waves.

Resumo

Nesta tese de mestrado, nós nos concentramos em cristais clássicos bidimensionais com interações suaves entre pares e a baixas temperaturas. Tipicamente, a rede triangular é a configuração que minimiza a energia potencial de interação. Tal energia é calculada através de um somatório de rede e nós mostramos algumas aproximações analíticas para ela. Nós estaremos interessados nos casos onde a densidade coarse-grained (a densidade "olhada de longe", abordada como contínua) depende levemente da posição. Isto pode ser causado por uma força externa nas partículas e, então, a suavidade das interações determinará como a densidade coarse-grained deve variar. No equilíbrio, este gradiente de densidade gerará uma força igual e oposta, resultante das interações. No limite de pequenos gradientes, o sistema tem poucos defeitos e conserva localmente a simetria de rede triangular. Embora a configuração do sistema tenha um enorme número de graus de liberdade, apenas a dependência da densidade coarse-grained com a posição é nossa informação relevante em escalas muito maiores que a distância entre primeiros vizinhos. Portanto, nós investigamos o cálculo da força resultante de interação devido a tais variações da densidade com a posição. Uma forma simples e intutitiva, mas não rigorosa, de obter a força da Teoria Dinâmica do Funcional de Densidade é mostrada. Além disso, uma abordagem microscópica que fornece o mesmo resultado é proposta. Vemos que, no equilíbrio, esta força fornece a minimização da energia livre total e tem sido bem sucedida em vários sistemas de não-equilíbrio. Mostramos que esta força falha no caso das ondas longitudinais de longo comprimento de onda, fornecendo um resultado menor para a velocidade do som. Em recentes simulações computacionais, nós obtivemos configurações de equilíbrio onde a mesma correção na força é necessária. Nós mostramos que tal correção pode ser obtida adicionando um termo de correção na energia livre, calculada como um funcional da densidade coarse-grained.

Palavras-chave: Matéria Condensada Frágil. Cristais Bidimensionais. Teoria Dinâmica do Funcional de Densidade. Ondas Sonoras.

List of Figures

Contents

CHAPTER 1

Introduction

This M.Sc. thesis investigates crystals, two-dimensional (2D) ones [1]. We are basically interested in theoretical approaches for evaluation of interaction forces between the particles through a macroscopic viewpoint (i.e., without knowing the exact positions of particles but only a coarse-grained density distribution of them). We will show that the functional dependence of this force with the coarse-grained density is not unique.

This chapter introduces the very notion of 2D crystals. We start with a historical background, on experiments and theory, and then show some analytical considerations for the interaction energy in a regular 2D lattice.

Crystals are used by mankind since the Ancient Egypt, China and Sumer. Characterizations of them were solely based on their outer morphology. Only in the 1910s, the inner structure of crystals could be seen for the first time, by X-ray diffraction patterns ideas of Max von Laue, with the precious help of Walter Friedrich and Paul Knipping [2]. Long before the X-ray experiments, the first conclusion that the inner structure of a crystal must be periodic came in 1781. And it came by accident, according to what is said to have happened. As the story goes, a prismatic calcite crystal slipped out Rene-Just Haüy hands and break into many pieces on the floor. By analyzing the fragments, Haüy realized that there exists crystallographic planes, along which crystals cleave. He elaborated a theory relating these planes [3] and the law of rational indices. Thereafter, Ludwig Seeber in 1824 and Gabriel Delafosse in 1840, independently, came up with the idea that the best description of a crystal is by an array of discrete points generated by defined translational operations (see the Nature Milestones in Crystallography, available from http://www.nature.com/milestones/crystallography). Many considerations about all the possible symmetries were made during the 19^{th} century and finally, in 1891, Arthur Shoenflies and Evgraf Fedorov [4, 5] catalogued a total of 230 space groups in 3D and 17 wallpaper groups in 2D.

1.1 Two-dimensional crystals: Great variety found in experiments

It may be strange to think about 2D crystals. But, in fact, they are very common nowadays. They can grow on liquids and solids, or even levitated by electromagnetic forces, and surfaces are their preferred media. The phenomenon of adsorption is a great responsible for this [1, 6, 7]. The first observations of such crystals were made by Langmuir in the 1920s in experiments with amphiphilic molecules (organic molecules with hydrophilic and lipophilic properties) on the liquid-gas interface in Langmuir films [1]. Interesting occurrences of 2D crystals are, for instance, Abrikosov's vortices in superconducting films [8, 9], electrons trapped at a liquid

helium surface [10] and graphene [11].

Figure 1.1 Monolayer of xenon atoms adsorbed on the (001) surface of graphite (from [12]).

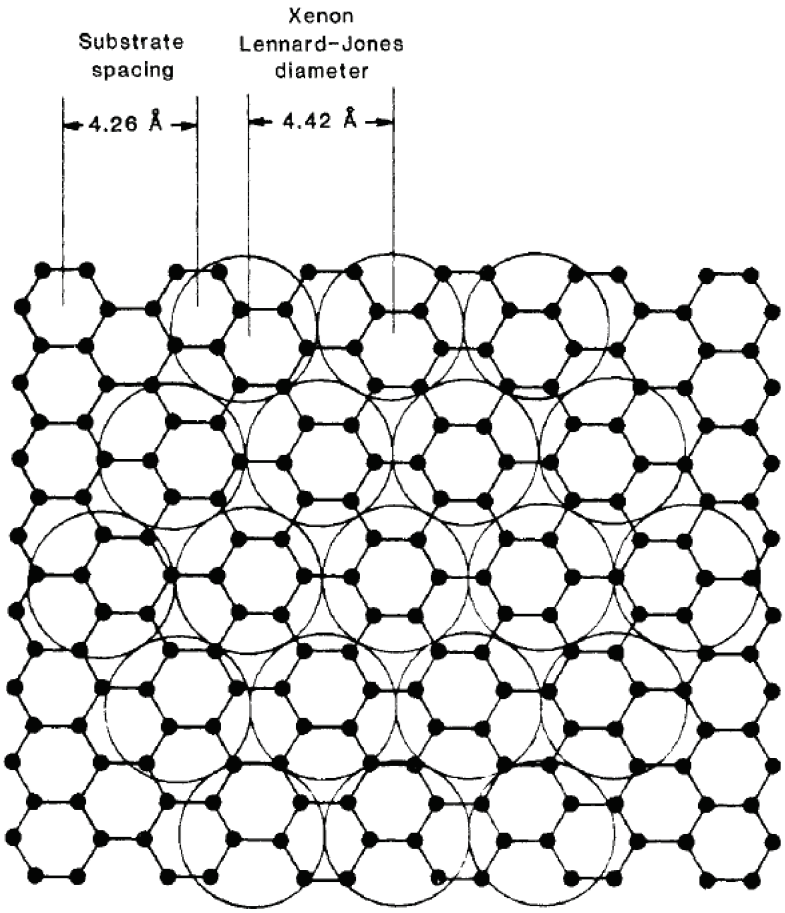

Figure 1.1 shows a monolayer of xenon adsorbed on the (001) basal plane surface of pyrolytic graphite. The interaction between xenon atoms can be approximated by Lennard-Jones type pairwise interaction ($V_p(r) = \varepsilon[(\sigma/r)^{12} - (\sigma/r)^6]$). We can see that the Lennard-Jones diameter is incommensurately larger than the separation between the relevant minima in the substrate potential of the graphite, i.e., the ratio between these distances is irrational. It has been shown that the graphite potential is weak and the system slightly differs from an ideal 2D system [12].

In this M.Sc. thesis, we are interested in inhomogeneities in the coarse-grained density of 2D crystals. Here we show some examples of them. In Figure 1.2, millimeter-sized steel balls are placed on a smooth aluminum substrate. Then, a few thousand volts are applied across the substrate and an electrically conductive cover [13, 14]. The balls, touching the aluminium, get instantaneously a mono-disperse charge and repel each other by Coulomb interaction. The substrate is slightly tilted in Figure 1.2 (b) so that the gravity acts, forming a density gradient.

Figure 1.2 Configuration of charged steel balls in a leveled (a) and tilted (b) substrate (from [13]).

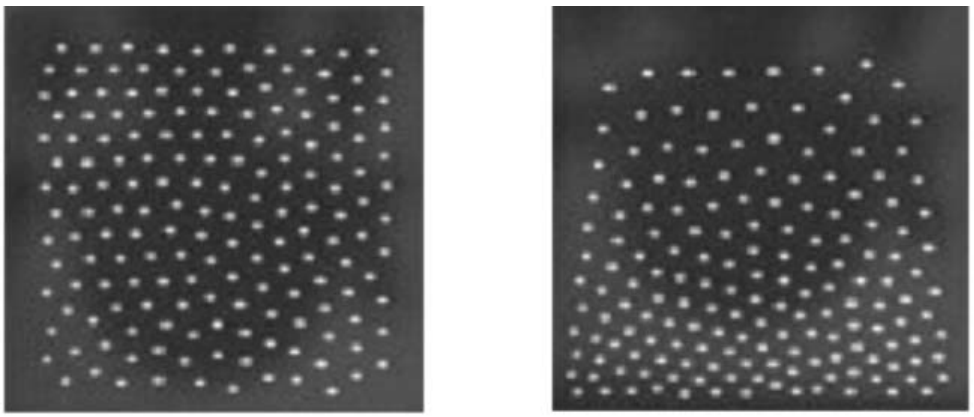

By knowing the gravitational force on each particle and their positions, one can find the net charge in each particle.

Figure 1.3 Configuration of magnetized steel balls in a tilted box. The "gravity rainbow" pattern (from [15]).

Steel balls and the influence of gravitational force are also used in the experiment of Figure 1.3, but the balls repel each other through a dipole-dipole interaction. They are placed within a flat box whose upper and lower walls were made of glass and a magnetic field is applied perpendicular to the box, inducing magnetic dipole moments [15]. The box is tilted and a density gradient appears, minimizing the energy (with the help of a delicate shaking). The pattern has arches remaining rainbows and it is known as "gravity rainbow".

In Figure 1.4, micrometer-sized dust melamine particles were dropped in an argon plasma exited by parallel-plate rf discharges. The dust particles charge negatively and form a levitated

Figure 1.4 Melamine particles dropped in radio frequency excited argon plasma (from [16]).

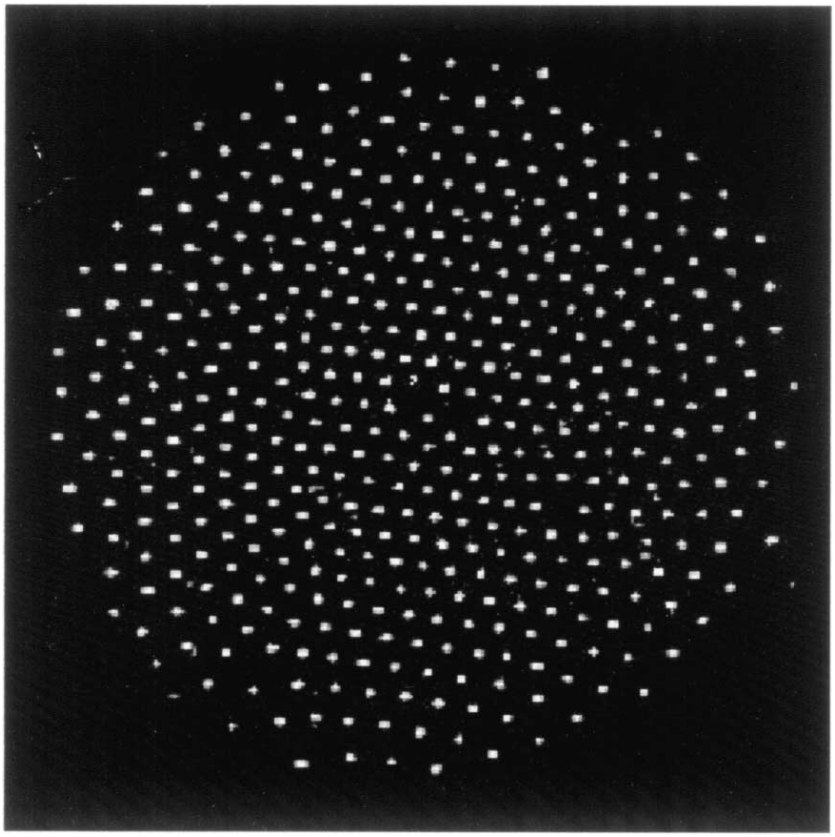

layer of particles where the electrostatic forces produced by the electrode plasma sheath counterbalance the gravity [16]. The vertical confinement is much stronger than the horizontal one. The interaction between the particles is approximately a Yukawa one. Theoretical approaches for this system will be seen in chapter 2.

1.2 Theory doubts their existence

The theoretical investigations on the existence of 2D crystals date back to the works of Landau [17] and Peierls [18] in the 1930s, where they proved the existence of a logarithmic divergence for the fluctuations of atomic displacements in a 2D system with continuous degrees of freedom. This implies an absence of ordered phase at any finite temperature. For the mean square fluctuation of a particle's position, we have

$$\langle \mathbf{u}^2 \rangle \sim \int \frac{d^2q}{q^2}, \tag{1.1}$$

due to thermal agitation caused by phonons. One can see that this integral converges in three dimensions (3D) and have a logarithmic divergence in 2D. Although they can exhibits Bragg

peaks in scattering experiments, no true long range order exists in 2D due to long wavelength fluctuations. This fact was sometimes used to argue the non-existence of 2D crystals and only systems of finite size might have crystal-like properties, since the logarithmic divergence in (1.1) is slow.

Figure 1.5 Illustration of formation and unbinding of a dislocation pair in a triangular lattice (from [19]).

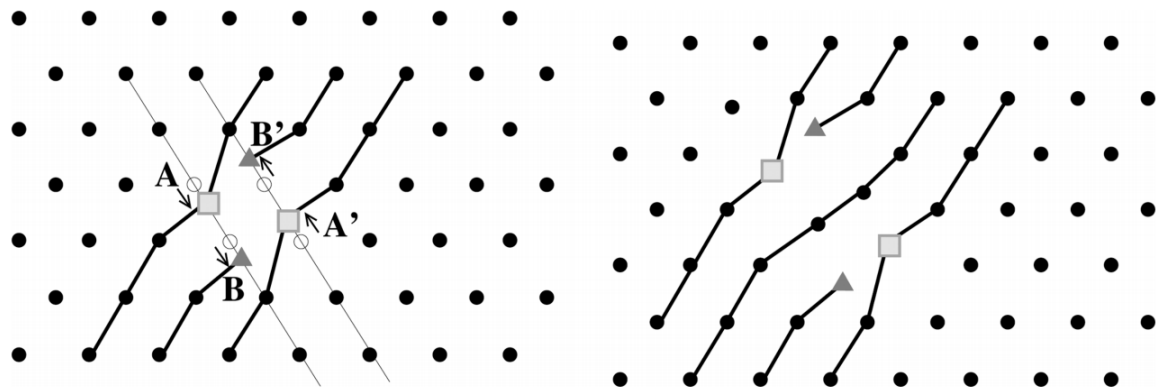

The famous Onsager's exact solution of a 2D Ising model in 1944 [20], showing long-range ordering, and the discovery of a liquid-solid transition for hard disks by Alder and Wainwright in 1962 [21], using numerical simulations, motivated several studies in the 1960s [22, 23, 24, 25, 26]. These studies (and other more rigorous [27, 28, 29]) showed that there cannot be a spontaneous breaking of continuous symmetry in 2D (a rigorous proof for translational invariance in hard disk systems only appeared in 2002, with Ioffe *et al.* [30]). But the rotational symmetry can be an exception.

Stanley and Kaplan in 1966 [31], by analyzing the extrapolation from high-temperature expansions, discovered that the susceptibility of the 2D XY model (which was proved to have no long-range order) diverged at some point. This suggests the intriguing idea of a phase transition without the onset of order. Then Kosterlitz and Thouless, in 1973 [32], came up with a new definition of order. A new phase transition accompanied by a change in "topological order". They tried to use these ideas in the 2D solid-liquid transition, considering the unbinding of topological defects. Halperin and Nelson [33, 34] and, independently, Young [35] dealt with some remaining complications and completed in 1979 the famous KTHNY theory for two-dimensional melting. This theory describes a two-stage melting. First, heating the crystal will produce more and more dislocations pairs and then, at some temperature, the heat starts to unbind them. In Figure 1.5, we can see the formation and unbinding of a dislocation pair [19]. The square (triangle) particles represent sevenfold (fivefold) disclinations and each pair of disclination with opposite sign is a dislocation. Second, at a bigger temperature, the heat starts to unbind the disclination pairs and the system melts. The phase between these two defect-unbinding transitions is called hexatic.

In summary, we nowadays know that 2D crystals have orientational long-range order (they do break rotational symmetry [36] and the shear modulus is nonzero) and translational quasi-long-range order (power-law decay of the correlation function of displacements). Suppose the equilibrium sites of the crystal lattice are $\mathbf{R}_i = n_i\mathbf{a}_1 + m_i\mathbf{a}_2$, where $\mathbf{a}_1$ and $\mathbf{a}_2$ are the primitive vectors and n_i and m_i are integers, and the instantaneous particles' positions are [25] $\mathbf{r}_i \equiv \mathbf{r}(\mathbf{R}_i) = \mathbf{R}_i + \mathbf{u}(\mathbf{R}_i)$. Then we have, as $|\mathbf{R}_i - \mathbf{R}_j| \to \infty$,

$$\langle [\mathbf{u}(\mathbf{R}_i) - \mathbf{u}(\mathbf{R}_j)]^2 \rangle \sim \ln |\mathbf{R}_i - \mathbf{R}_j|, \tag{1.2}$$

and

$$\langle [\mathbf{r}(\mathbf{R}_i + \mathbf{a}_1) - \mathbf{r}(\mathbf{R}_i)] \cdot [\mathbf{r}(\mathbf{R}_j + \mathbf{a}_1) - \mathbf{r}(\mathbf{R}_j)] \rangle \tag{1.3}$$

goes to a constant.

In 3D, the components of the displacement field $\mathbf{u}(\mathbf{r})$, roughly defined by $\mathbf{r}_i \equiv \mathbf{r}(\mathbf{R}_i) = \mathbf{R}_i + \mathbf{u}(\mathbf{R}_i)$, are the Nambu-Goldstone modes corresponding to the translational symmetry broken in each coordinate of space. Therefore, they are "hydrodynamic modes", i.e., collective modes characterized by slowly relaxation toward their equilibrium values. These modes can come from conservation laws or, in the case of ordered systems, from continuous broken symmetries [37]. Even though there is no genuine long-range translational ordering in 2D, Ziuppelius *et al.* [38] considered the displacement field as hydrodynamic modes (the modes correspondent to the rotational broken symmetry are not independent, but slaved to the displacement field) since it relax slowly. For finite systems at very low temperatures, the 2D crystal can then be viewed as a static lattice. This allows us to study many important mechanical properties using two simple theoretical aspects: the energy and force due to interparticle interactions in a triangular lattice.

We will ignore the displacement field and consider the coarse-grained density as our relevant hydrodynamic mode. The properties present in crystals and absent in liquids will only modify the energy dependency with density. This is done by considering the local triangular lattice symmetry. We will concentrate on these aspects in the present thesis and consider classical interactions. Examples of mechanical properties to be explored are the sound speed velocity [39, 40] and the equilibrium inhomogeneous coarse-grained density profile [41, 42].

The operation of coarse-graining in density was first introduced by Paul and Tatiana Ehrenfest [43, 44], a century ago, as a result of density averaging in cells. The size of cells is assumed to be small, but finite, and does not tend to zero. In fact, it is much smaller than the macroscopic scales and much bigger than interparticle distances. We will consider that the inhomogeneity of coarse-grained density is small, with a predominant triangular symmetry and few defects. In this case, the coarse-grained density is related with the mean interparticle distance (mean nearest-neighbor distance) trough the geometry of triangular lattice.

The triangular lattice is the highest-density lattice arrangement. Due to this fact, it is by far the most common arrangement in two-dimensions. This is evident when the hamiltonian (energy) decrease in a close packing of particles (as in interactions with an attractive part and a hard core), i.e., in a more dense system. On the contrary, if there are repulsive interactions and the system is confined at a given density, triangular lattice will provide the greatest nearest-neighbor distance.

1.3 Interaction Energy of a lattice (Madelung energy)

The total interaction energy of a single particle i of a lattice, also known as the Madelung energy, is calculated by the sum

$$\phi = \sum_{j \neq i} V_p(\mathbf{r}_i - \mathbf{r}_j), \tag{1.4}$$

where $\mathbf{r}_i$ and $\mathbf{r}_j$ are the positions of particles i and j, respectively, and $V_p(\mathbf{r}_i - \mathbf{r}_j)$ is the pairwise interaction potential. We will consider identical particles (one-component crystal) and only isotropic pair potentials, i.e., $V_p(\mathbf{r}_i - \mathbf{r}_j) = V_p(|\mathbf{r}_i - \mathbf{r}_j|)$.

In two-dimensions, power-law interactions $V_p(r) = q^2/r^m$ will result in convergence of ϕ if $m > 2$. In a two-component crystal, with positive and negative charges, the sum in equation (1.4) can still have a conditional convergence if $m \leq 2$. A Coulomb potential $V_p(r) = q^2/r$ and alternating positive and negative charges in the lattice give rise to the famous Madelug Constants, represented by conditionally convergent lattice sums.

1.3.1 Continuum approximation and self-interaction correction

When the interaction has some range λ, and $V_p(r) = V_p(r/\lambda)$, and the nearest-neighbors' distance x is much smaller than λ, each particle sees the others in a coarse-grained way. In other words, we do not need the exact particle positions in other to calculate ϕ with a good precision, wich already obtained with only their mean distribution in big scales, i.e. the coarse-grained density ρ. Then we have the continuum approximation

$$\phi \approx 2\pi\rho \int_0^\infty dr r V_p(r). \tag{1.5}$$

In a triangular lattice, the relation between ρ and x can be obtained geometrically, which gives $\rho = 2/(\sqrt{3}\mathrm{x}^2)$.

The continuum approximation has some kind of self-interaction. It integrates over the whole plane, covering every lattice site, but the particle at $r = 0$ must not be included in the evaluation of ϕ (equation (1.4)). The circle with Wigner-Seitz radius $r_{WS} = 1/\sqrt{\pi\rho}$ is a good representation of the region to be avoided in integrating equation (1.5). A self-interaction correction can then be obtained by

$$\phi \approx 2\pi\rho \int_{r_{WS}}^\infty dr r V_p(r). \tag{1.6}$$

1.3.2 Nearest-neighbors approximation and a crossover method

If the interaction range is very small, only the nearest-neighbors (which are six in triangular lattice) have relevant contribution in equation (1.4) and then we can use the nearest-neighbors' approximation

$$\phi \approx 6V_p(\mathrm{x}). \tag{1.7}$$

In order to obtain a simple procedure to obtain approximations for ϕ, which works well for both limit cases of long and short-range of interaction, given by equations (1.5) and (1.7), we

proposed a method in [45]. Such a method can be applied for $1D$, $2D$ and $3D$ lattices. We will here present it for a $2D$ lattice.

The Madelung Energy related to a single test particle is the total potential energy due to the interaction between the test particle and the rest of the lattice. Figure 1.6 shows a schematic representation of a regular lattice where the test particle was chosen to be the central particle (see closed black circle within the central white circular region in Figure 1.6).

Figure 1.6 Schematic representation of a $2D$ lattice where particles are indicated by closed dark circles. The reference particle is located in the center of the figure within the white circle. The first three most internal annuli A_0, A_1 and A_2 are indicated, respectively, by the decreasing gray darkness regions. (From [45].)

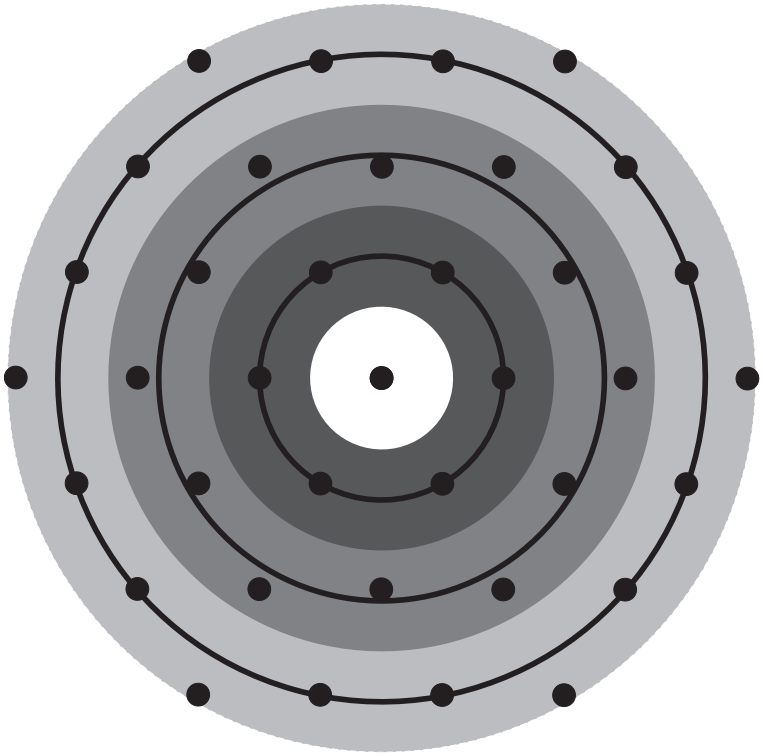

The method is as follows: we divide the plane of the $2D$ lattice in a set of concentric annuli denoted by A_n $(n = 0, 1, 2, ...)$ of same thickness equal to y and with average radii $r_n = r_0 + n$y. The first (A_0), second (A_1) and third (A_2) annuli are represented, respectively, by decreasing gray darkness regions in Figure 1.6.

Concerning the first annulus, A_0, we request the following two conditions to be satisfied: 1) the average radius r_0 of the annulus A_0 must have the value x, and 2) the total charge within the annulus A_0 must be equal to Nq, where N is the total number of nearest-neighbors of the lattice (number of particles at the distance x from the test particle).

The total charge Q_n of a given annulus A_n, in the continuous limit, is given by

$$Q_n = \int_{A_n} \rho q dA = 2\pi\rho q \int_{r_n - \mathrm{y}/2}^{r_n + \mathrm{y}/2} r dr = 2\pi\rho q \mathrm{y} r_n. \tag{1.8}$$

The value of y can be obtained by using the second requirement concerning the first annulus, which results in the equation

$$N = \int_{A_0} \rho(\mathrm{x}) dA = 2\pi\rho \int_{r_0 - \mathrm{y}/2}^{r_0 + \mathrm{y}/2} r dr, \tag{1.9}$$

where $r_0 = \mathrm{x}$, and then

$$\mathrm{y} = \frac{N}{2\pi\rho\mathrm{x}}. \tag{1.10}$$

For the last step of our method, we consider that the total charge of the annulus A_n is uniformly distributed over a ring of radius r_n, which is the average radius of the annulus. In doing so, we obtain an approximative expression for the Madelung Energy, given by

$$\phi(\mathrm{x}) = \sum_{n=0}^{\infty} \frac{Q_n}{q} V_p(r_n). \tag{1.11}$$

Notice that the expression depends on the lattice's topology via the number of nearest neighbor particles N and the density of particles ρ.

The Yukawa potential $V_p(r) = q^2 e^{-\kappa r}/r$ (a shielding in the Coulomb potential) has an interaction range determined by the parameter κ. Yukawa lattices appear in a variety of physical systems [46, 47, 16]. The method equation (1.11) for triangular Yukawa lattices gives the good closed-form approximation

$$\phi(\mathrm{x}) = 6q^2 \frac{e^{-\kappa'}}{\mathrm{x}(1 - e^{-\frac{3\sqrt{3}}{2\pi}\kappa'})}, \tag{1.12}$$

where $\kappa' = \kappa\mathrm{x}$. Figure 1.7 (a) shows a plot of the Dimensionless Madelung Energy (DME) $\varphi(\kappa') = \kappa \mathrm{x}^2 \phi(\mathrm{x})/q^2$ obtained numerically, by the self-interaction correction (equation (1.6)), by the nearest-neighbors approach (equation (1.7)), by the method (equation (1.12)) and by the approximation used in [48]. The relative error is showed in Figure 1.7 (b). We can see that it goes to zero in the continuum and nearest-neighbors asymptotic limits, $\kappa' \to 0$ and $\kappa' \to \infty$ respectively. Its maximum value is less than 0.5%. This relative error is well fitted by the function

$$E_t(\kappa') = \frac{c\kappa'^2}{e^{d\kappa'} - 1}, \tag{1.13}$$

where $c = 0.00462$ and $d = 0.8016$ (see full line in Figure 1.7 (b)). Finally, by using the latter fit to improve the accuracy of equation (1.12), we obtain the following expression

$$\varphi_t^{imp}(\kappa') = \frac{\varphi_t(\kappa')}{1 - E_t(\kappa')}. \tag{1.14}$$

The maximum relative error of this semi-analytic approximation is expressively reduced to a value smaller than 0.0007%

1.4 Summary of the Chapter

In this introductory chapter, we review a historical background about crystals, focusing on 2D ones. Experimental examples and an elementary discussion about the theoretical notion of 2D crystals at finite temperatures were given. Finally, analytical approximations for the interaction force of a lattice, which is essentially different from the liquid case, were shown in the light of the results of a paper we previously published [45].

The next chapter presents the case of a two-dimensional Yukawa cluster where the crystalline structure influence the calculation of energy and force, especially at the edge. Thus, we found good results for the coarse-grained density profile. These were the results of another published paper [42].

Figure 1.7 (a) Dimensionless Madelung Energy (DME) $\varphi(\kappa') = \kappa x^2 \phi(x)/q^2$ of the triangular lattice obtained numerically (circles) and by different analytical approaches as indicated within figure. (b) Relative error $E_t(\kappa') = |\varphi_{exact} - \varphi_{method}|/\varphi_{exact}$ (circles), between the DME calculated analytically by our method (equation (1.12)) and numerically, and fit of the error (equation (1.13), full line), as a function of the parameter κ'. Both figures have the horizontal axis in the same logarithmic scale. (From [45].)

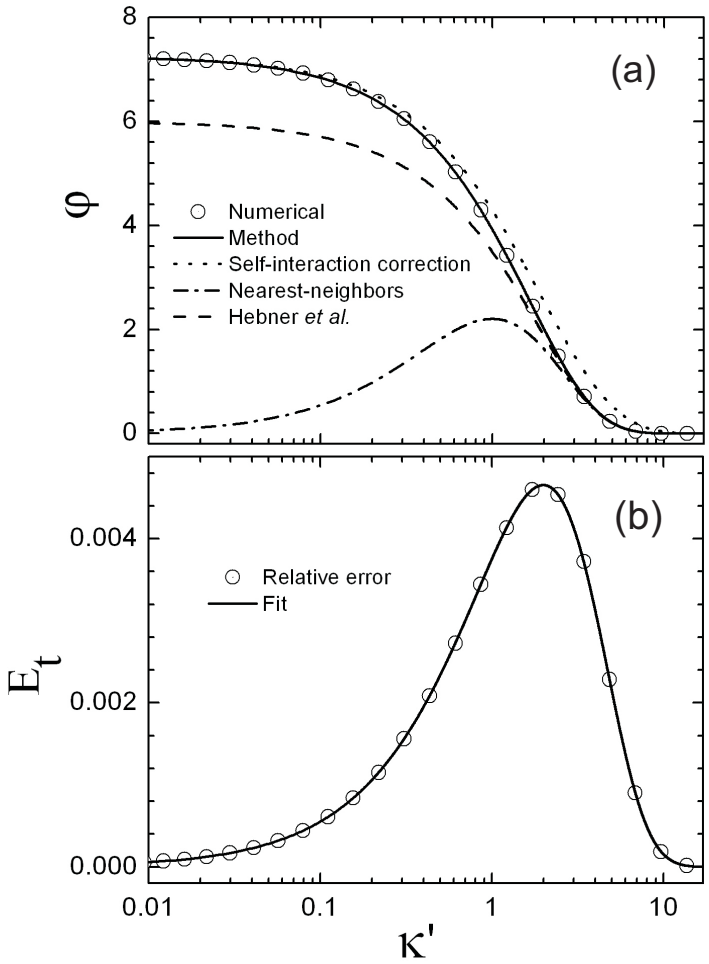

CHAPTER 2

Continuum theory for two-dimensional complex plasma clusters

In the previous chapter we introduced some notions about classical two-dimensional crystals and their interaction energy at the zero temperature limit, considering perfect lattices.

External forces on the crystal can provoke a inhomogeneous coarse-grained density, i.e., a position dependent $\rho(\mathbf{r})$. These forces are counterbalanced by an interaction force associated with the density gradient $\nabla\rho(\mathbf{r})$.

The present chapter shows entirely the manuscript we published in the New Journal of Physics [42], with minor modifications, in accordance with the Creative Commons Attribution 3.0 Unported (CC-BY) license (https://creativecommons.org/licenses/by/3.0/). It investigates the complex plasma cluster. An important example of classical two-dimensional crystals with inhomogeneous coarse-grained density. Some approaches, including a new proposed one, to the calculation of interaction force are shown. All approaches for the force reduce to the same result for the approximations used here. But the differences between the density functional approach and the proposed one will be important in the rest of this thesis. Here, our consideration of Finite Size Effects (FSE) and of the force at the edge of the system are crucial for the accuracy in the final results.

2.1 Introduction

In complex (dusty) plasma, monodisperse microspheres of dust can be made to float in a circular monolayer. Electrostatic and gravitational forces are used to confine them vertically. With radial confinement and low temperature, the particles form finite crystalline clusters [49, 50]. The radial potential well is approximately parabolic and is responsible for the circular shape of the cluster. The interaction between dust particles in the plasma is typically subject to shielding by electrons and ions and is therefore frequently described by the Yukawa (or Debye-Hückel) interaction [47, 51].

It is hoped that, given the external potential's parameter, the spatial particle distribution obtained from an experiment or simulation can give values for the interparticle potential parameters by using a suitable theoretical model [52]. In isotropically confined three-dimensional ($3D$) systems [53, 54], much research has been made toward this direction. The behaviors of the density distribution for many particles [55, 56] and of the shells' structures for few particles (the so called Yukawa/Coulomb Balls) [57] follow well known phenomenological and ab initio equations. These theories give a good accuracy in almost the entire range of the parameters. In $2D$ large systems with moderate and strong screening, the continuum density profile was

obtained with a satisfactory accuracy [52, 41, 48]. However, the density profile or the system's radius for relatively small number of particles (8-500) and for weak screening (or strong confinement) were not well predicted theoretically.

There are other methods for determination of interaction parameters in Yukawa systems (see, e.g., [58]) but macroscopic properties, such as density and radius, can also be investigated in other two-dimensional systems, and a same procedure can be used in many of them. For instance, similar studies were made in systems with pure Coulomb [59], dipolar [60] and superconductor vortex-vortex [61] interactions.

In this letter, we derive good approximations for the density and the radius of $2D$ complex plasma clusters. The local density approximation with finite size effects, which were not considered previously in $2D$, was used for the interaction energy. By considering deformations in the triangular lattice, which is the predominant symmetry in the system, a new differential equation for the spatial dependence of density is obtained. The general form of this differential equation is different from the ones obtained from others approaches used in the literature [52, 41, 48]. The procedure to obtain this equation help us to find a new boundary condition which, with the necessary careful considerations, is essential to the accuracy of the final equation. We compare the theory with results of MD simulations and find that it has a surprisingly good accuracy for a great range of the number of particles N, even when the density cannot be considered continuum ($8 < N < 500$). Moreover, from simulations we found that this system has two regimes where the system's size and density profile are the same but the interaction parameters are different.

Formally, the paper is structured as follows. In the next section the model system and details concerning the MD simulations are given. In Section 2.3, our theoretical approach is developed and, in Section 2.4, their results are compared with those obtained from simulations. Finally, Section 2.5 contains a summary of the main results.

2.2 Model

With a Yukawa type pair potential $V_{pair}(r_{ij}) = q^2 e^{-\kappa r_{ij}}/r_{ij}$ and an external potential $V_{ext}(r) = V_0 r^2/2$, the Hamiltonian of the system is given by

$$H = \frac{1}{2}\sum_{i}^{N}\sum_{j\neq i}^{N}\frac{q^2 e^{-\kappa|\mathbf{r}_i-\mathbf{r}_j|}}{|\mathbf{r}_i-\mathbf{r}_j|} + \sum_{i}^{N}\frac{V_0 r_i^2}{2} \tag{2.1}$$

$$= \frac{q^2\kappa}{2}\sum_{i}^{N}\left[\sum_{j\neq i}^{N}\frac{e^{-\kappa|\mathbf{r}_i-\mathbf{r}_j|}}{\kappa|\mathbf{r}_i-\mathbf{r}_j|} + \frac{(\kappa r_i)^2}{\alpha}\right], \tag{2.2}$$

where N is the number of particles, q is the dust charge, κ is the screening parameter, V_0 is the confining potential parameter and $\alpha = \kappa^3 q^2/V_0$. The rescaled particles' radial positions κr_i at the ground state are determined uniquely by α and N.

To search for equilibrium configurations of this system, we use a simulated annealing scheme. This is summarized as follows: first, for a given set of parameters, particles are placed

at random positions and the solvent is set at a high initial temperature. Then, the solvent temperature is slowly decreased down to $T = 0$ at a constant rate. The time evolution of the system at a temperature T is modeled by overdamped Langevin equations of motion. These are integrated via Euler finite difference steps following the algorithm

$$\mathbf{r}_i(t+\Delta t) = \mathbf{r}_i(t) + \mathbf{F}_i(t)\Delta t + \mathbf{g}\sqrt{2T\Delta t}, \tag{2.3}$$

where $\mathbf{F}_i(t) = -\sum_j \nabla_i V_{pair}(r_{ij})$ is the total force applied to the particle, Δt is the time step and the components of the two-dimensional vector $\mathbf{g}$ are independent random variables with standard normal distribution which accounts for the Langevin kicks.

2.3 Theoretical Development

2.3.1 Interaction Energy and the Local Density Approximation

In a continuum approximation for the particle density $\rho(\mathbf{r})$, the total potential over a particle located at $\mathbf{r}$ is given by

$$\phi(\mathbf{r}) = \int_{r' \leq R_m} \rho(\mathbf{r}') \frac{q^2 e^{-\kappa|\mathbf{r}-\mathbf{r}'|}}{|\mathbf{r}-\mathbf{r}'|} d^2 r', \tag{2.4}$$

where R_m is the system's radius. When the range of the potential, $1/\kappa$, is small compared to the system size (i.e., when $\kappa R_m \gg 1$), a small region around $\mathbf{r}$ gives the main contribution to the integral of equation (2.4). In this case, the effective region of integration is approximately a circle with radius of the order of $1/\kappa$ and centered at the position vector $\mathbf{r}$. For such a circular symmetry in the region of integration, we can expand $\rho(\mathbf{r}')$ around $\mathbf{r}$ (that is, $\rho(\mathbf{r}') = \rho(\mathbf{r}) + (\mathbf{r}'-\mathbf{r})\cdot\nabla\rho(\mathbf{r}) + |\mathbf{r}'-\mathbf{r}|^2\nabla^2\rho(\mathbf{r})/4 + \ldots$) and one can see that the second term vanishes in the integral of $\rho(\mathbf{r}')e^{-\kappa|\mathbf{r}-\mathbf{r}'|}/|\mathbf{r}-\mathbf{r}'|$. Therefore, the use of just the first term, i.e., of the local density $\rho(\mathbf{r})$, may give a good approximation for $\phi(\mathbf{r})$. This is called the local density approximation (LDA).

On the other hand, when R_m is equal to a few units of $1/\kappa$ or less, finite size effects (FSE) must be considered. These effects were taken into account only in the $3D$ case by C. Henning *et al.* [56] and we will use a similar FSE consideration in $2D$. Even with a constant density, the integral of equation (2.4) cannot be given in terms of elementary functions. In this case, we consider a position independent FSE by simply integrating over the region $|\mathbf{r}'-\mathbf{r}| \leq R_m$, i.e., a disk of radius R_m centered at $\mathbf{r}$, which gives

$$\phi(\mathbf{r}) = \phi(\rho(\mathbf{r})) = \rho(\mathbf{r}) \int_{|\mathbf{r}'-\mathbf{r}|\leq R_m} \frac{q^2 e^{-\kappa|\mathbf{r}-\mathbf{r}'|}}{|\mathbf{r}-\mathbf{r}'|} d^2 r' = \frac{2\pi q^2 \rho(\mathbf{r})}{\kappa}(1 - e^{-\kappa R_m}). \tag{2.5}$$

As the system has locally a predominant triangular lattice symmetry, the density is related to the nearest particles' distance x by $\rho = 2/(\sqrt{3}\mathrm{x}^2)$. In the limit of strong screening, i.e., a big value of κ and therefore a short range of the pair potential, each particle effectively interacts only with its nearest-neighbors. In this case, the total potential $\phi(\mathbf{r})$ is approximately equal to 6 (the number of nearest-neighbors of the triangular lattice) times $V_{pair}(\mathrm{x}(\mathbf{r}))$.

Now we make the consideration that each particle in the cluster always interacts with only six effective particles at a distance x (see Figure 2.1 (a)) through an effective potential given by $V_{eff}(\mathrm{x}) = \phi(\mathrm{x})/6$, even when the interaction has a long-range character. In fact, each effective particle is in a nearest-neighbor position but represents the interaction with all the particles in one sixth of the system as is shown in Figure 2.1 (a). In the short-range case, the effective potential becomes the pair potential and the effective particles become the nearest-neighbor particles. We considered that the total potential over a particle can be given explicitly in terms of x, i.e., $\phi(\mathbf{r}) = \phi(\rho(\mathbf{r})) = \phi(\mathrm{x}(\mathbf{r}))$, which is always true for the LDA without a position dependent FSE.

Equation (2.5) is a continuum approximation and therefore it is accurate only when the interaction range $1/\kappa$ is much bigger than the particles' spacing x ($\kappa\mathrm{x} \ll 1$). In fact, for Yukawa systems, this approximation fails when $\kappa\mathrm{x} \gg 1$, or even $\kappa\mathrm{x} \sim 1$ [45], and one should consider correlation (discretization) effects. In this case, each particle interacts, effectively, only with few particles in its neighborhood. As those particles have a triangular lattice-like arrangement, we approximate their interaction energy by that given by a perfect triangular lattice. A good approximation for this energy was obtained in [45] by summing up a set of well-defined rings. To include the FSE, we must perform the sum up to the ring of radius $\approx R_m$, which yields

$$\phi(\mathrm{x}) = \frac{6q^2 e^{-\kappa \mathrm{x}}}{\mathrm{x}\left(1 - e^{-\frac{3\sqrt{3}}{2\pi}\kappa \mathrm{x}}\right)}\left(1 - e^{-\kappa R_m}\right). \tag{2.6}$$

Notice that in the regime of $\kappa\mathrm{x} \ll 1$ (or $\rho/\kappa^2 \gg 1$) the equation (2.5) is recovered. In the rest of this letter, we will use equation (2.5) and concentrate on $10^{-4} \leq \alpha \leq 10^{1}$. Nevertheless, the already good results obtained for average and great values of α ($\propto \kappa^3$) [41, 48] can still be further improved by using equation (2.6).

Figure 2.1 (a) Effective particles and their respective sixth part of the plane. (b) Relative positions of the effective particles in the presence of an external force $\mathbf{F}_{ext} = -V_0 r\hat{\mathbf{r}}$.

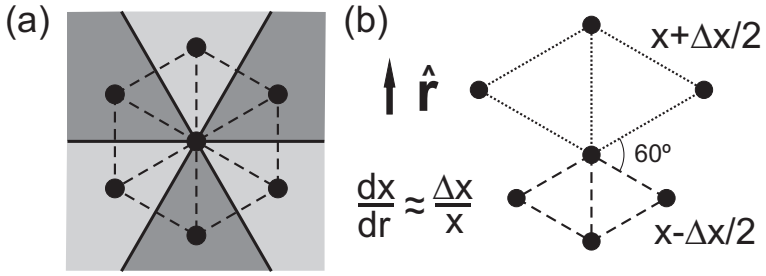

2.3.2 Differential equation for the density

In order to compensate the external force, $\mathbf{F}_{ext} = -V_0 r\hat{\mathbf{r}}$, one must consider a deformation of the original hexagon formed by the effective particles. To do so, we choose the dislocation shown in Figure 2.1 (b). In this case, the distance between the central particle and the three effective

particles in the positive (negative) direction of $\hat{\mathbf{r}}$ was increased (decreased) by $\Delta x/2$. The angle between two neighbor particles remains $\pi/3$ and the total potential remains the same up to the first order in Δx.

The magnitude of the force due to an effective particle is $F(x) = -\frac{\partial V_{eff}}{\partial x} = -\frac{1}{6}\frac{\partial \phi}{\partial x}$. Therefore, from Figure 2.1 (b) and from the equilibrium of forces, we have

$$(1+2\cos(\pi/3))\,[F(x-\Delta x/2) - F(x+\Delta x/2)] = V_0 r, \tag{2.7}$$

which, for small Δx, becomes

$$-2\frac{\partial F}{\partial x}\Delta x = V_0 r. \tag{2.8}$$

For a smooth dependence of x with r we associate $\Delta x/x$ to the derivative of x with respect to r. This is based on the fact that the variation of the nearest-neighbor distance from the bottom rhombus to the top one, i.e., the difference between their sides, in Figure 2.1 (b), is Δx and the radial distance between their centers is x. By substituting $\Delta x = x(dx/dr)$ in equation (2.8), we obtain the following differential equation

$$\frac{x}{3}\frac{\partial^2 \phi}{\partial x^2}\frac{dx}{dr} = V_0 r. \tag{2.9}$$

This last equation written in terms of the density becomes

$$\left(\frac{\partial \phi}{\partial \rho} + \frac{2}{3}\rho\frac{\partial^2 \phi}{\partial \rho^2}\right)\nabla\rho + \nabla V_{ext} = 0, \tag{2.10}$$

where $V_{ext}(\mathbf{r})$ represents a general external potential.

The obtained differential equation has a general form different from other well-known approaches. In a variational approach [41], the minimization of the total potential energy functional

$$U[\rho] = \frac{1}{2}\int_{r\leq R_m} \rho(\mathbf{r})\phi(\rho(\mathbf{r}),\mathbf{r})d^2r + \int_{r\leq R_m} \rho(\mathbf{r})V_{ext}(\mathbf{r})d^2r, \tag{2.11}$$

under the constraint $\int \rho(\mathbf{r})d^2r = N$, gives

$$\frac{1}{2}\nabla\left(\phi + \rho\frac{\partial \phi}{\partial \rho}\right) + \nabla V_{ext} = 0. \tag{2.12}$$

Whilst in a hydrostatic approach [48], the Euler equation

$$\frac{\nabla P}{\rho} + \nabla V_{ext} = 0, \tag{2.13}$$

where $P = -\partial(\phi/2)/\partial(1/\rho) = (\rho^2/2)\partial\phi/\partial\rho$ is the pressure, gives

$$\frac{1}{\rho}\nabla\left(\frac{\rho^2}{2}\frac{\partial \phi}{\partial \rho}\right) + \nabla V_{ext} = 0. \tag{2.14}$$

In spite of the differences between equations (2.10), (2.12) and (2.14), by using an approximation for ϕ of the form $\phi(\mathbf{r}) = B\rho(\mathbf{r})$, where B is a constant, they provide the same result for the density, i.e., $\rho(\mathbf{r}) = \rho_0 - V_{ext}(\mathbf{r})/B$ where ρ_0 is a constant of integration. The differences between these equations appear when ϕ has other dependencies with ρ and $\mathbf{r}$. These differences will be investigated in future work. Now we use the result $\rho(\mathbf{r}) = \rho_0 - V_{ext}(\mathbf{r})/B$ together with the approximation of equation (2.5) and the external potential $V_{ext}(r) = V_0 r^2/2$ to obtain the following equation for the density

$$\frac{\rho(r)}{\kappa^2} = \frac{\rho(0)}{\kappa^2} - \frac{\kappa^2 r^2}{4\pi\alpha\left(1 - e^{-\kappa R_m}\right)}. \tag{2.15}$$

The values of $\rho(0)/\kappa^2$ and κR_m are obtained from the boundary and normalization conditions. As remarked in Section 2.2, they must depend only on the parameters α and N.

2.3.3 Boundary and normalization conditions

A continuum approximation for the density must satisfy the normalization condition $\int \rho(\mathbf{r}) d^2 r = N$, which in our case is written as

$$2\pi \int_0^{R_m} \rho(r) r dr = N. \tag{2.16}$$

This equation can be used to eliminate one unknown term of equation (2.15), while the second one can be eliminated from a boundary condition.

The most simple boundary condition is to say that $\rho(R_m) = 0$. However it does not indeed happen, although becomes a good approximation in the large N limit where, as observed in experiments and simulations, $\lim_{N\to\infty} \rho(R_m)/\rho(0) = 0 \ \forall\alpha$. The use of this condition and equation (2.16) in equation (2.15) gives

$$\frac{\rho(\kappa r)}{\kappa^2} = \frac{\kappa^2 R_m^2 - \kappa^2 r^2}{4\pi\alpha\left(1 - e^{-\kappa R_m}\right)}, \tag{2.17}$$

where

$$\frac{(\kappa R_m)^4}{\alpha(1 - e^{-\kappa R_m})} = 8N. \tag{2.18}$$

Except by the factor $(1 - e^{-\kappa R_m})$ descendant from FSE, this result was obtained by H. Totsuji *et al.* [41] by using a variational approach. There, the result $\rho(R_m) = 0$ comes out from the minimization of the total energy obtained from the LDA without FSE and correlation effects. When the latter effects were considered [41], a nonzero density at the edge came out naturally, satisfying $\lim_{N\to\infty} \rho(R_m)/\rho(0) = 0$.

Notice that, from the effective particles approach of Figure 2.1 (b), a straightforward boundary condition appears. When the central particle of Figure 2.1 (b) is at the boundary of the cluster, the three effective particles at the top do not exist. Therefore, the equilibrium of forces considered in equation (2.7) is now written as $(1 + 2\cos(\pi/3))F(\mathrm{x}_m) = V_0 R_m$, where x_m is the nearest-neighbor distance at the boundary, or equivalently

$$-\frac{1}{3}\frac{\partial\phi}{\partial \mathrm{x}}\Big|_{\mathrm{x}_m} = V_0 R_m. \tag{2.19}$$

Despite the consideration of just 3 effective particles in this case, the effective potential continues to be given by $\phi(\mathrm{x})/6$. This is in fact a correction for our choice of the term $(1-e^{-\kappa R_m})$ for the FSE. This choice overestimates the potential at the edge by a factor that approximates the number 2 as κR_m increases.

By placing the potential ϕ of equation (2.5) into (2.19), we obtain an expression relating x_m and R_m

$$-\frac{1}{3}\left[\frac{-8\pi q^2}{\sqrt{3}\kappa \mathrm{x}_m^3}\right]\left(1-e^{-\kappa R_m}\right) = V_0 R_m. \tag{2.20}$$

Figure 2.2 A particle located at the edge of the system has only a half of its hexagonal Wigner-Seitz cell inside the circle of radius R_m.

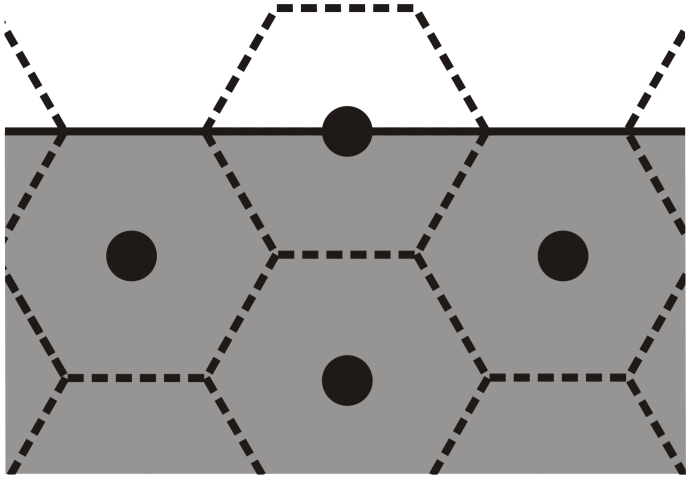

An important and non-trivial consideration must be made here: for a particle at the edge, just a fraction of its Wigner-Seitz cell is inside the circle of radius R_m (see Figure 2.2). This fraction is approximately one half for $R_m/\mathrm{x}_m > 1$. Due to this fact, the density (given by the inverse of Wigner-Seitz cell area) at the edge is related to x_m by

$$\rho(R_m) = \frac{4}{\sqrt{3}\mathrm{x}_m^2}. \tag{2.21}$$

This correction in the density should be made always that the superior limit of integration of the normalization condition shown in equation (2.16) is R_m. In this case, the total area occupied by all Wigner-Seitz cells must be equal to πR_m^2 but it is overestimated if we always have $A_{WS} = 1/\rho = \sqrt{3}\mathrm{x}^2/2$ (see equation (2.2)). This problem has not been considered previously in the literature but it becomes important in small systems. Equation (2.21) is not exact but gives a good approximation to correct this problem.

Using equations (2.21) and (2.20), we obtain

$$\frac{\rho(R_m)}{\kappa^2} = \sqrt{3}\left(\frac{\kappa R_m}{\pi\alpha\left(1-e^{-\kappa R_m}\right)}\right)^{2/3}. \tag{2.22}$$

The above equation is one of the main theoretical results obtained in this article. It will be determinant for the good accuracy of the theory at small number of particles. By using equation (2.22) in (2.15), we can find $\rho(0)$ in terms of R_m. Finally, the density at any point is then given by

$$\frac{\rho(\kappa r)}{\kappa^2} = \sqrt{3}\left(\frac{\kappa R_m}{\pi\alpha\left(1-e^{-\kappa R_m}\right)}\right)^{2/3} + \frac{\kappa^2(R_m^2-r^2)}{4\pi\alpha\left(1-e^{-\kappa R_m}\right)}, \tag{2.23}$$

where κR_m can be found by using equation (2.16), which gives

$$\sqrt{3}\left(\frac{\sqrt{\pi}(\kappa R_m)^4}{\alpha\left(1-e^{-\kappa R_m}\right)}\right)^{2/3} + \frac{(\kappa R_m)^4}{8\alpha(1-e^{-\kappa R_m})} = N. \tag{2.24}$$

2.3.4 Scale invariance

For a given number of particles, equations (2.23) and (2.24) inform that the distances in the system scale with R_m, i.e.,

$$\rho(r) = R_m^{-2} f(N, r/R_m), \tag{2.25}$$

where $f(N, r/R_m)$ is independent on the potentials' parameters. This would imply that the values of κ and α cannot be obtained separately from the final configuration of an experiment, but only from a relation between them. Another experiment with a different N must be done in order to get a new relation.

A density profile obeying equation (2.25) can be obtained when the potential ϕ is, up to a constant, approximated by $\phi(\mathbf{r}) = B\rho(\mathbf{r})$. By using this approximation, the method of the previous two subsections (i.e., any of equations (2.10), (2.12) and (2.14) together with $\rho(R_m) = 4/(\sqrt{3}x_m^2)$ and equation (2.19)) gives

$$R_m^2\rho(r) = f(N, r/R_m) = \sqrt{3}c^2 + \frac{c^3}{4}\left(1 - \frac{r^2}{R_m^2}\right), \tag{2.26}$$

where $c = c(N)$ is obtained from

$$c^3 + 8\sqrt{3}c^2 = 8N/\pi, \tag{2.27}$$

and R_m is related to B by

$$2V_0R_m^4 = Bc^3. \tag{2.28}$$

The factor B can be a function of N, R_m and of the potentials' parameters; and may be obtained, for example, by: (a) an integral of the pairwise potential $B = \int V_p(r)d^2r$, as it was done in equation (2.5), or (b) by a derivative of the Madelung energy (equation (2.6)), $B = \partial\phi/\partial\rho$, evaluated at the mean density $\bar{\rho} = N/\pi R_m^2$. Indeed, the approximation $\phi = B\rho$ is very general and can be used in many systems beyond Yukawa [61, 62], and so does equations (2.26) and (2.27).

The scale invariance of the theory is broken when position dependent FSE (small κR_m) or correlation effects (small ρ/κ^2) are taken into account. Using the latter, C. Totsuji *et al.* [63] were able to obtain approximate values of κ and q^2, for a given V_0, by considering the α-dependence of $R_m^2\rho(0)$. Their results are applicable with the assumption that $\alpha \gg 1$. But, as we will see in Section 2.4, if all values of α are possible *a priori*, α can be a bi-valued function of $R_m^2\rho(0)$.

2.4 Results

Equations (2.24) and (2.26) for the radius and the density, respectively, developed in the latter section, were compared with the results obtained from Molecular Dynamics simulations in order to verify the accuracy of our theory.

We defined the system's radius as the radial distance of the outermost particle. Although, in the theory, we have made considerations that demand great values of κR_m and ρ/κ^2, which implies in the need of great number of particles since $N = \pi R_m^2 \bar{\rho}$, we still found satisfactory results even for $N < 500$. Figure 2.3 (a) shows the N-dependence of κR_m, obtained from equation (2.24) (lines) and simulations (symbols) for $\alpha = 10^1$, 1, 10^{-1}, 10^{-2}, 10^{-3} and 10^{-4}. In Figure 2.3 (b), we compare equation (2.24), equation (2.24) using $\rho(R_m) = 2/(\sqrt{3}\mathrm{x}_m^2)$ instead of (2.21), equation (2.18) and the equations obtained in [48] and [41] (with cohesive energy) in the case of $\alpha = 10^{-2}$. It can be seen the great improvement obtained for small systems by using the boundary condition of equation (2.22).

The surprisingly good agreement of the theory for small number of particles is evidenced in Figure 2.4 where $\alpha = 10^{-2}$ and no logarithm scale is used. The dotted and dashed lines represent equations (2.18) and (2.24), respectively. One can see that the boundary condition of equation (2.22) was responsible for a great improvement in the theory.

The inset of Figure 2.4, which is a zoom for $2 < N < 21$, shows that, although the radius obtained from simulations is discontinuous for small N, the theory gives a good smooth approximation. A good accuracy starts as $N > 8$, when the structural transition $(1,7) \mapsto (2,7)$ occurs for all α [64]. For $N \leq 8$, the particles are located at the vertices of a regular polygon centered at the origin with one or none particle at the center. In these cases, the exact values of κR_m can be easily obtained theoretically. For $\alpha = 10^{-2}$, the relative error of equation (2.24) is less than 5% for any $N > 8$.

The radial density profile was calculated by dividing the system in annuli and counting the number of particles in each annulus. This number is then divided by the area of the respective annulus and this is taken as the density at the mean radius of the annulus. For a smooth profile, the width of the annuli cannot be too small. Such smoothness can only be obtained for $N \gtrsim 100$.

Since the accuracy of the theory for the radius is already known from Figure 2.3, we now investigate the accuracy for the density by showing only how $R_m^2\rho$ depends on r/R_m. By doing this, the scale invariance predicted by the theory in Section 2.3.4 is also investigated.Figure 2.5 shows $R_m^2\rho$ versus r/R_m for many values of α (the same of Figure 2.3 (a)) and for (a) $N = 10000$, (b) $N = 1000$ and (c) $N = 100$. In the figure is shown the results from our theory, which is given by equation (2.26) and does not depend on α, and from the one developed in [41] (with cohesive energy) for $\alpha = 10^{-4}$ and $\alpha = 10^1$ (the curves for other values of α are between the two and so are the ones obtained by the theory of [48]). As it can be seen, our theory gives a good approximation even for values of N between 100 and 1000, which are more easy to be achieved in experiments.

We can see from figures 2.5(a) and 2.5(b) that the density behavior is approximately parabolic and depends on α. We interpolate this density using a one-parameter fitting function given by

$$R_m^2\rho = \frac{2N}{\pi(2-d)}\left(1 - d\frac{r^2}{R_m^2}\right), \tag{2.29}$$

where $d = d(\alpha, N)$ is the fitting parameter. This function is parabolic on r and attends the conditions of equation (2.16) and of continuity of its gradient for $|\mathbf{r}| < R_m$. Figure 2.6 (a) shows the values of d for $N = 10000$ as a function of α obtained by interpolations of equation (2.29) with simulation results (symbols) compared with the value predicted by the theory (line). We can see that the fitting results have a well-behaved dependence on α. However, it is not injective, i.e., it does not have a one-to-one correspondence. For instance, the scaled densities of $\alpha = 10^{-4}$ and $\alpha = 10^{5}$, for $N = 10000$, are shown in Figure 2.6 (b) and one can see that they are almost the same. This implies in a limitation of any theory for the density: there can be two possible values for each of the system's parameters (κ, q and V_0) which can result in the same values of R_m and $\rho(r)$ coming from an experiment or simulation. Also, just a theory which accounts non-local, finite size and correlational effects can predict these two regimes at the same time, giving the two possible values of the parameters.

2.5 Conclusions

The density profile and the system's size of $2D$ complex plasma clusters confined by a parabolic potential are obtained analytically. For the calculation of the interaction energy, we used the LDA with a position independent FSE. A differential equation for the density was obtained by a new method. By using the proposed interaction energy, this differential equation gives the same result of the variational [41] and pressure [48] approaches, however our method gives light to an important new boundary condition.

The density resulted from our approximation scales with the radius, implying that the values of κ and α cannot be calculated separately from the final configuration of a single experiment. In fact, the real density does not have this scale invariance but it is showed that there are systems with different α but identical normalized density profiles.

The boundary condition and the FSE were determinant to provide surprisingly good results in systems with relatively small number of particles ($8 < N < 500$). For instance, for $\alpha = 10^{-2}$, the relative error of the theoretical maximum radius is less than 5% for any $N > 8$.

2.6 Summary of the Chapter

We investigated a system where a great number of particles interact via Yukawa interaction and are trapped in a parabolic well (generating an external force which is linear with the distance from the center). The interaction energy was approximated by the continuum approach with inclusion of finite size effects. A simple method to find the force is proposed and edge effects were considered, providing good results.

The proposed method will be further developed in the next Chapter and we will see that it provides the same result of Density Functional Theory.

Figure 2.3 (a) Scaled radius κR_m versus number of particles N in logarithm scale obtained from simulations (symbols) and equation (2.24) (lines) for $\alpha = 1$, 10^{-1}, 10^{-2}, 10^{-3} and 10^{-4}. (b) Comparison between our theoretical results and the ones developed in [48] and [41].

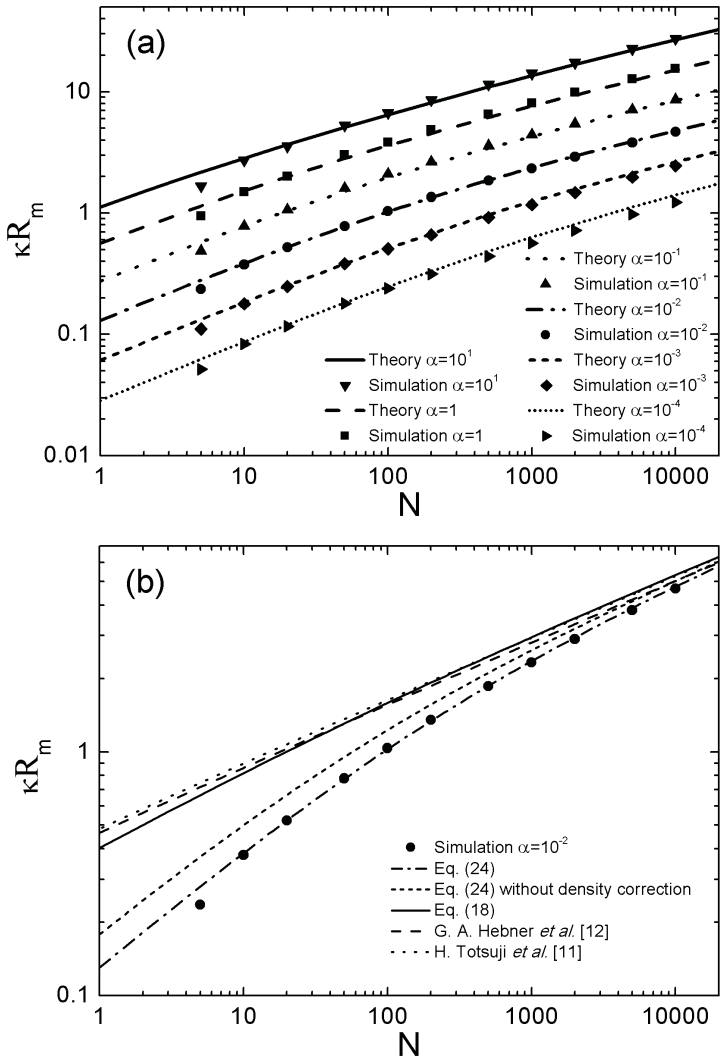

Figure 2.4 Scaled radius κR_m versus number of particles N in normal scale for $\alpha = 10^{-2}$ obtained by equation (2.24) (dashed line), equation (2.18) (dotted line) and by simulations (symbols). The inset shows a zoom for $2 < N < 21$.

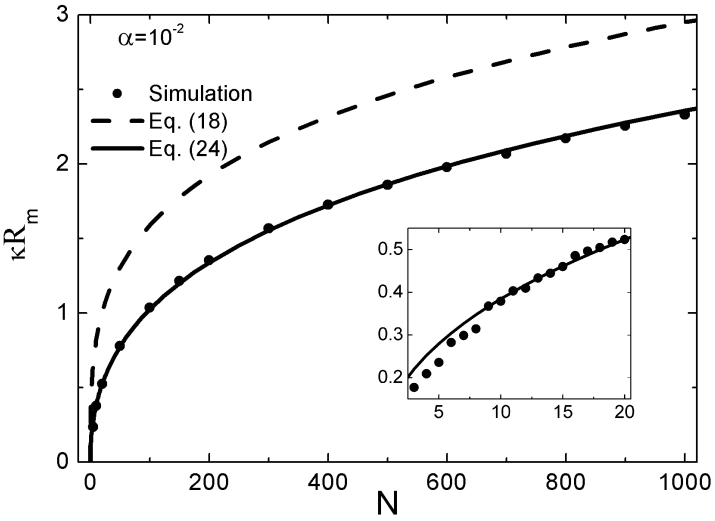

Figure 2.5 Scaled density $R_m^2\rho$ versus scaled radial distance r/R_m obtained by the theory (line) and by simulations (symbols) for several values of α and (a) $N = 10000$, (b) $N = 1000$ and (c) $N = 100$.

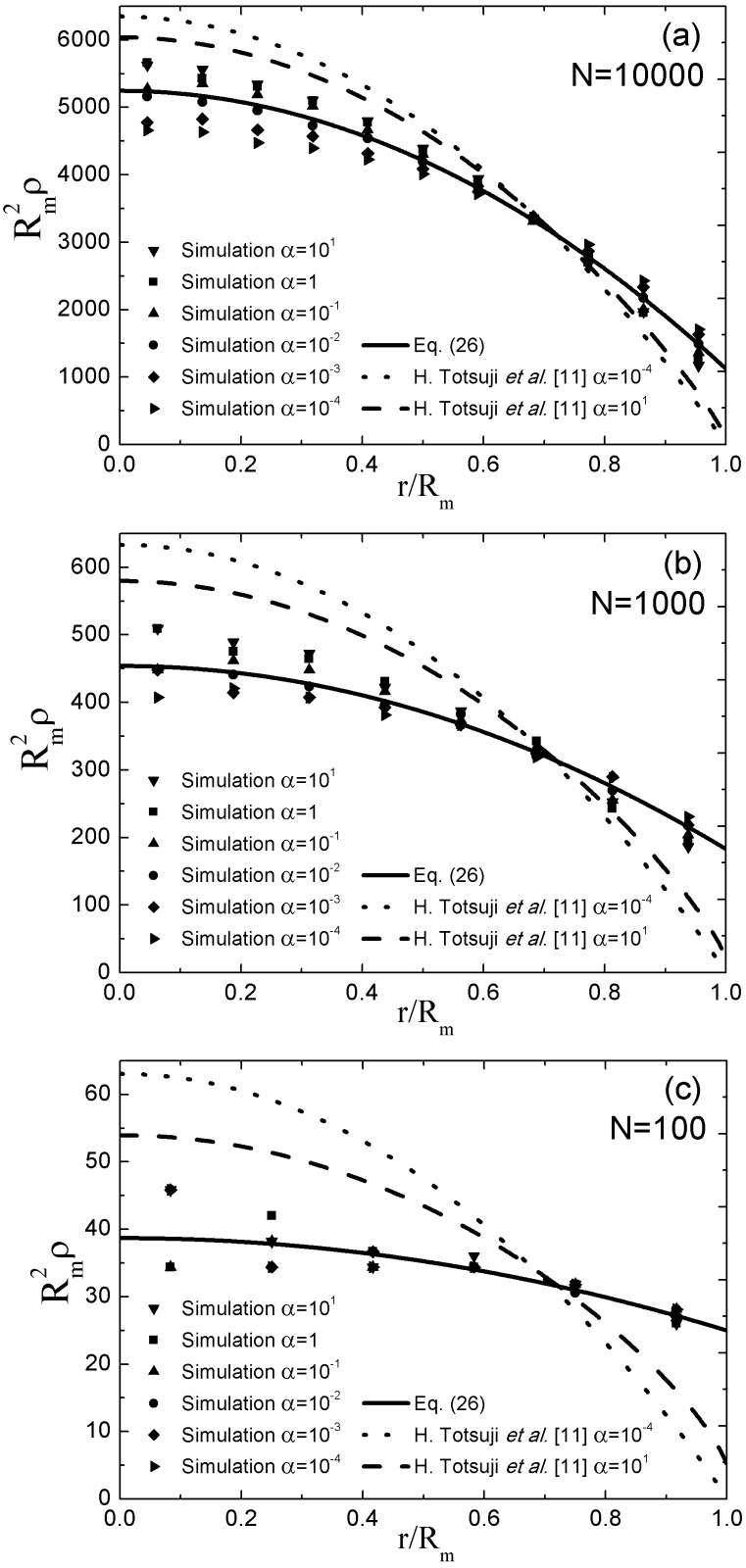

Figure 2.6 (a) Coefficient d versus α obtained by interpolations (symbols) and by theory (horizontal line). (b) Scaled density $R_m^2\rho$ versus r/R_m obtained from simulations for $\alpha = 10^{-4}$ and $\alpha = 10^5$.

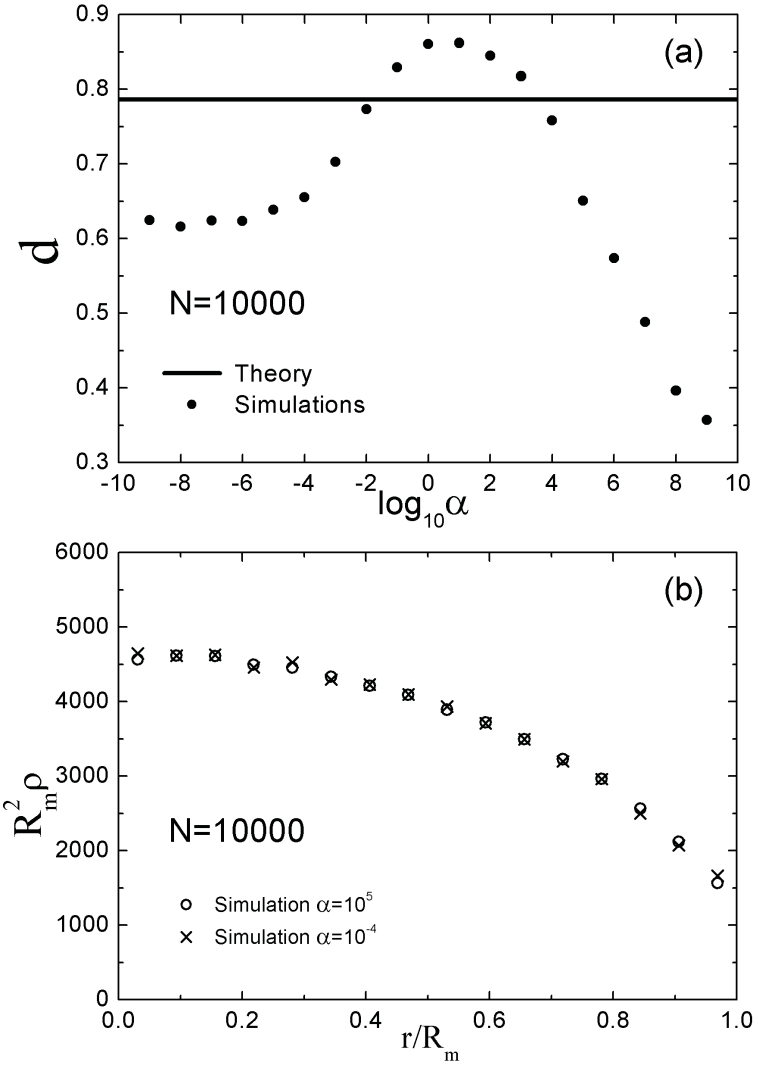

CHAPTER 3

DDFT force due to density gradient in 2D crystals

The Dynamical Density Functional Theory (DDFT) to nonequilibrium statistical mechanics has been successfully applied to many systems (see [65, 66, 67, 68, 69] and references therein). Despite the success of the theory, it rests upon an adiabatic approximation. Within such approach, it is assumed that the nonequilibrium two-body correlations are approximately equal to those of an imagined equilibrium situation with the same instantaneous one-body density distribution $\hat{\rho}(\mathbf{r},t)$ [68, 70]. Before we show the DDFT result for the force, lets present some definitions.

The one-body density distribution is related to the probability distribution of particle positions at time t, $P(\mathbf{r}_1,\mathbf{r}_2,...,\mathbf{r}_N,t) \equiv P(\{\mathbf{r}_i\},t)$, by

$$\hat{\rho}(\mathbf{r}_1,t) = N \int d^2r_2 d^2r_3 ... d^2r_N P(\{\mathbf{r}_i\},t), \tag{3.1}$$

or, equivalently,

$$\hat{\rho}(\mathbf{r},t) = \sum_i^N \langle \delta(\mathbf{r}-\mathbf{r}_i)\rangle. \tag{3.2}$$

Moreover, the probability distribution $P(\{\mathbf{r}_i\},t)$ is related to the statistical phase-space distribution function $f(\{\mathbf{r}_i\},\{\mathbf{p}_i,\},t)$ by a integration in phase space

$$P(\{\mathbf{r}_i\},t) = \int d^2p_1 ... d^2p_N f(\{\mathbf{r}_i\},\{\mathbf{p}_i,\},t), \tag{3.3}$$

where $\{\mathbf{p}_i\}$ stand for the momenta. Also, we can define the pair density distribution by

$$\hat{\rho}^{(2)}(\mathbf{r}_1,\mathbf{r}_2,t) = N(N-1)\int d^2r_3 ... d^2r_N P(\{\mathbf{r}_i\},t) = \sum_{i,j}^{N\,\prime} \langle \delta(\mathbf{r}-\mathbf{r}_i)\delta(\mathbf{r}-\mathbf{r}_j)\rangle, \tag{3.4}$$

where the prime indicates that the sum goes over $i \neq j$, and then define the conditional distribution by $\hat{\rho}(\mathbf{r}_2|\mathbf{r}_1,t) = \hat{\rho}^{(2)}(\mathbf{r}_1,\mathbf{r}_2,t)/\hat{\rho}(\mathbf{r}_1,t)$, which is the average particle density at $\mathbf{r}_2$ given a particle fixed at $\mathbf{r}_1$. Notice that, at low temperatures and finite time scales, $\hat{\rho}(\mathbf{r},t)$ approximates to a sum of sharp gaussians and then it differs from the coarse-grained density.

3.1 Density Functionals

Classical Density Functional Theory (DFT) [71] splits the grand potential into four contributions of one-body density functionals,

$$\mathscr{F}[\hat{\rho}] = \mathscr{F}_{id}[\hat{\rho}] + \mathscr{F}_{ex}[\hat{\rho}] + \int d^2r \hat{\rho}(\mathbf{r}) V_{ext}(\mathbf{r}) - \mu \int d^2r \hat{\rho}(\mathbf{r}), \tag{3.5}$$

where $V_{ext}(\mathbf{r})$ is the external potential, μ is the chemical potential, $\mathscr{F}_{id}[\hat{\rho}] = k_B T \int d^2 r \hat{\rho}(\mathbf{r})[\ln \Lambda^3 \hat{\rho}(\mathbf{r}) - 1]$ is the exact ideal gas contribution and $\mathscr{F}_{ex}[\hat{\rho}]$ is the excess part of Helmholtz free energy due to interparticle interactions. At zero temperature, $\mathscr{F}_{id} = 0$ and $\mathscr{F}_{ex}$ is expected to be simply the total potential energy of interparticle interactions. Equilibrium DFT [68] says that the total interaction force on a particle is given by

$$\mathbf{F}(\mathbf{r}) = -\int d^2 r_2 \hat{\rho}(\mathbf{r}_2|\mathbf{r}_1)\nabla_1 V_p(r_{12}) = -\nabla \frac{\delta \mathscr{F}_{ex}[\hat{\rho}(\mathbf{r})]}{\delta \hat{\rho}}. \tag{3.6}$$

In the next section we show a simple but non-rigorous derivation of this force in the limit of low temperatures. The assumption that equation (3.6) remains valid in nonequilibrium is the so-called adiabatic approximation assumed in DDFT [68]. It is equivalent to assuming that the pair density $\hat{\rho}^{(2)}(\mathbf{r}_1, \mathbf{r}_2, t)$ relaxes instantaneously to the equilibrium pair-density corresponding to the current one-body density $\hat{\rho}(\mathbf{r}_1, t)$. The DDFT force then has the same form of equation (3.6), together with equation (3.5), adding temporal dependence labels.

In the limit of zero temperature, small inhomogeneity and short-range interaction on the crystal, we can use the Local Density Approximation (Section 2.3) and the interaction and the external potential energy can be expressed as functionals of the coarse-grained density $\rho(\mathbf{r})$ (which results from a coarse-graining of $\hat{\rho}(\mathbf{r})$), given by

$$U_{int}[\rho] = \frac{1}{2}\int \rho(\mathbf{r})\phi(\rho(\mathbf{r}))d^2 r \tag{3.7}$$

and

$$U_{ext}[\rho] = \int d^2 r \rho(\mathbf{r}) V_{ext}(\mathbf{r}), \tag{3.8}$$

respectively. $\phi(\rho(\mathbf{r}))$ is the Madelung Energy, given by the lattice sum of equation (1.4).

Our main objective is this thesis is to investigate if, for some suitable coarse-grained density functional $\mathscr{F}_{ex}[\rho]$, the force given by equation (3.6) is still valid in the limits described above. And if this suitable excess free energy functional is exactly the interaction potential energy (equation (3.7)).

3.2 Simple intuitive but non-rigorous derivation of DDFT force

Consider, at time t, a dislocation of particle i of the system from $\mathbf{r}_i(t)$ to $\mathbf{r}_i(t) + d\mathbf{r}$. We assume the approximation that other particle positions remain unchanged and the variation in density, for low temperatures, is given by $\delta\hat{\rho}(\mathbf{r}, t) \approx \delta(\mathbf{r} - \mathbf{r}_i(t) - d\mathbf{r}) - \delta(\mathbf{r} - \mathbf{r}_i(t))$. Then, the variation in the total free energy is given by

$$\begin{aligned} \delta\mathscr{F} &= \int d^2 r \frac{\delta \mathscr{F}}{\delta \hat{\rho}}[\hat{\rho}(\mathbf{r}, t)]\delta\hat{\rho}(\mathbf{r}, t) \\ &= \frac{\delta \mathscr{F}}{\delta \hat{\rho}}[\hat{\rho}(\mathbf{r}_i(t) + d\mathbf{r}, t)] - \frac{\delta \mathscr{F}}{\delta \hat{\rho}}[\hat{\rho}(\mathbf{r}_i(t), t)]. \end{aligned} \tag{3.9}$$

The force on particle i at $\mathbf{r}_i$ will be the negative of variation in energy, in the direction where it is maximum, divided by $|d\mathbf{r}|$ in the limit where this goes to zero. Therefore, from equation (3.9), we obtain the same result of equation (3.6).

3.3 Microscopic approach

The same force of equation (3.6) can be obtained in a microscopic approach of interparticle interactions. This can be achieved in a better investigation of the approach proposed in Section 2.3.2.

Lets start from zero. Consider a classical two-dimensional crystal with triangular lattice symmetry and particles interacting via an isotropic pairwise potential $V_p(r_{ij})$. Consider also that the effective range of $V_p(r_{ij})$ is of the order of x (the nearest neighbor's distance of the crystal).

Let a particle of this triangular lattice be at the origin with its six neighbors at $\{\mathbf{r}_i\}$ ($i = 1,2,...,6$), as is shown in Figure 3.1 (a). We have $|\mathbf{r}_i| = |\mathbf{r}_{i+1} - \mathbf{r}_i| = \mathrm{x}_0$ where x_0 is the nearest-neighbors' distance, related to the coarse-grained particle density ρ_0 by $\rho = 2/(\sqrt{3}\mathrm{x}^2)$. Also, let θ_1^0 and $\theta_{i+1}^0 = \theta_i^0 + \pi/3$ be the angles between $\mathbf{r}_i$ and some axis $\hat{\mathbf{y}}$ (see Figure 3.1 (a)).

Now, consider a perturbation on this lattice such that a small density gradient antiparallel to $\hat{\mathbf{y}}$ is formed, as is shown in Figure 3.1 (b). The nearest-neighbors' distances have now a position dependence $\mathrm{x} = \mathrm{x}(\mathbf{r})$. This gradient provokes deformations in the crystal (deformations in $\{\mathbf{r}_i\}$) and now we have angle perturbations $\delta\theta_i = \theta_i - \theta_i^0$ and perturbations in the twelve nearest-neighbors' distances $\delta\mathrm{x}_i = \mathrm{x}_i - \mathrm{x}_0$ and $\delta\mathrm{x}'_i = \mathrm{x}'_i - \mathrm{x}_0$, which are given by $\mathrm{x}_i = |\mathbf{r}_i|$ and $\mathrm{x}'_i = |\mathbf{r}_{i+1} - \mathbf{r}_i|$ and are defined at the mean positions of their neighbors, i.e., $\mathbf{r}_i/2$ and $(\mathbf{r}_{i+1} + \mathbf{r}_i)/2$, respectively. We are considering the case of a particle with 6 neighbors far from lattice defects. Topological lattice defects are inevitable, in general, in a inhomogeneous system but important to locally sustain a triangular lattice symmetry [72].

To be more precise in what we mean by a small density gradient, consider that the relative variations in the nearest-neighbors's distances shown in Figure 3.1 (b) are small. In other words, $\delta\mathrm{x}_i/\mathrm{x}_0$ and $\delta\mathrm{x}'_i/\mathrm{x}_0 \ll 1$ for all i, and since the denominator is of the order of the distances between the positions where x_i and x'_i are defined, we have $|\nabla\mathrm{x}| \ll 1$, or

$$|\nabla\rho| \ll \rho^{3/2}, \tag{3.10}$$

to be satisfied in the crystal.

If the particles interacts with short-range pairwise repulsive potential $V_p(r)$, the total force $\mathbf{F} = F\hat{\mathbf{y}}$ on the origin particle due to its neighbors, after the perturbation, will no longer be zero. Instead, it will be given by

$$\begin{aligned} F &= \sum_{i=1}^{6} V_p'(\mathrm{x}_i)\cos\theta_i \\ &= V_p''(\mathrm{x}_0)\sum_{i=1}^{6}\delta\mathrm{x}_i\cos\theta_i^0 - V_p'(\mathrm{x}_0)\sum_{i=1}^{6}\delta\theta_i\sin\theta_i^0, \end{aligned} \tag{3.11}$$

up to first order in perturbations. Notice that the perturbations $\delta\mathrm{x}'_i$ relates $\delta\mathrm{x}_i$ and $\delta\theta_i$ by $\delta\mathrm{x}'_i = (\delta\mathrm{x}_i + \delta\mathrm{x}_{i+1})/2 + \sqrt{3}\mathrm{x}_0(\delta\theta_{i+1} - \delta\theta_i)/2$.

The density gradient $\nabla\rho$ is a coarse-graining definition and so is $\nabla\mathrm{x}$. If such gradient is formed infinitely slowly, the system can adapt its configuration remaining close to equilibrium.

Figure 3.1 (a) A particle and its 6 neighbors in a perfect triangular lattice. The angles θ_i are defined from the direction of $\hat{\mathbf{y}}$ (b) Deformations in the lattice forming a density gradient antiparallel to $\hat{\mathbf{y}}$.

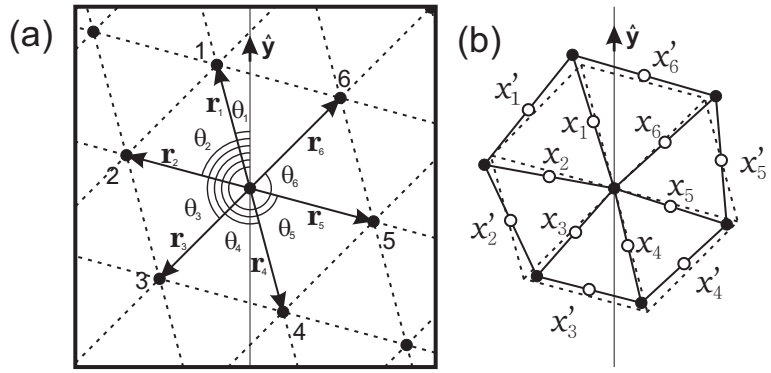

Then the microscopic variations of x_i and x'_i in Figure 3.1 (b) obey $\nabla\mathrm{x}$, even in such a small scale. Then we have

$$\mathrm{x}_i = \mathrm{x}_0 + \nabla\mathrm{x}\cdot\frac{\mathbf{r}_i}{2} \Rightarrow \delta\mathrm{x}_i = \frac{\mathrm{x}_0\cos\theta_i^0|\nabla\mathrm{x}|}{2}, \tag{3.12}$$

and

$$\mathrm{x}'_i = \mathrm{x}_0 + \nabla\mathrm{x}\cdot\frac{(\mathbf{r}_i+\mathbf{r}_{i+1})}{2} \Rightarrow \delta\mathrm{x}'_i = \frac{\sqrt{3}\mathrm{x}_0\cos(\theta_i^0+\pi/6)|\nabla\mathrm{x}|}{2}. \tag{3.13}$$

These equations give $\sum_{i=1}^{6}\delta\mathrm{x}_i\cos\theta_i^0 = 3\mathrm{x}_0|\nabla\mathrm{x}|/2$ and $\sum_{i=1}^{6}\delta\theta_i^0\sin\theta_i^0 = 3|\nabla\mathrm{x}|/2$. Realize that $\mathrm{x}_0 = \sum_{i=1}^{6}\mathrm{x}_i/6 = \sum_{i=1}^{6}\mathrm{x}'_i/6$. Equation (3.11) then becomes

$$\mathbf{F} = \frac{3}{2}\left[\mathrm{x}_0 V_p''(\mathrm{x}_0) - V_p'(\mathrm{x}_0)\right]\nabla\mathrm{x}. \tag{3.14}$$

By a change of variables and considering that the force acts on a particle at $\mathbf{r}$, where $\mathrm{x}_0 = \mathrm{x}(\mathbf{r})$ is the average of its nearest-neighbors' distances, equation (3.14) can be written as

$$\mathbf{F}(\mathbf{r},t) = -\left[\frac{d\phi(\rho(\mathbf{r},t))}{d\rho} + \frac{\rho(\mathbf{r},t)}{2}\frac{d^2\phi(\rho(\mathbf{r},t))}{d\rho^2}\right]\nabla\rho(\mathbf{r},t), \tag{3.15}$$

where $\phi(\rho) = 6V_p(\mathrm{x}(\rho))$ is the total potential energy in the limit of short range.

In Section 2.3 we used the notion that the neighbor particles can act as effective particles, carrying the total interaction of the whole sixth part of the lattice they represent. The triangular lattice is made of a collection of hexagons with different orientations, where the particles are in their vertices, and we can use the same procedure presented above for all of them, since the result is independent of the direction $\hat{y}$. The total result for the force of the entire is the same of equation (3.15) where $\phi(\rho)$ is a lattice sum, with contributions of second and farther neighbors. The same result obtained from the consideration of effective particles.

The procedure described above, resulting in equation (3.15), gives the same force obtained from equation (3.6) where the free energy is simply the interaction potential energy

$$\mathscr{F}[\rho(\mathbf{r},t)] = U[\rho(\mathbf{r},t)] = \frac{1}{2}\int\rho(\mathbf{r},t)\phi(\rho(\mathbf{r},t))d\mathbf{r}, \tag{3.16}$$

where the Madelung energy $\phi = \phi(\rho) = \phi(\mathrm{x})$ is given by the lattice sum

$$\phi = \sum_i V_p(r_i) = \sum_i V_p(\mathrm{x}p_i), \tag{3.17}$$

where $p_i = r_i/\mathrm{x}$ depends only on the crystal's lattice symmetry. Notice that, in the limits of short range interaction, where $\phi(\rho) = 6V_p(\mathrm{x}(\rho))$, and small density gradient (equation (3.10)) used in the present case, the local density approximation can be used and equation (3.16) becomes exact.

3.4 Summary of the Chapter

This Chapter showed some approaches to find the interaction force acting in a particle in the crystalline state. The first and second sections do not needed to use any crystalline property. Although Section 3.3 used the triangular lattice geometry, the result obtained was the same (inside the limitations of validity). The next Chapter will present cases where the force assumes a different dependence with the coarse-grained density.

CHAPTER 4

Residual free energy

The nonequilibrium case of long wavelength longitudinal waves contains small density gradients, obeying equation (3.10), but we will see that the force given by equation (3.15) does not provide the correct result for the velocity of these waves, i.e,, for the crystal's sound speed. The correction for the force comes from an additional term in the free energy. We then construct a simple equilibrium case where the same correction is needed.

4.1 Long wavelength longitudinal waves (sound waves)

For the analysis of wave spectra (see, e.g., [39]), consider the continuity,

$$\frac{\partial \rho}{\partial t} + \nabla \cdot (\rho \mathbf{v}) = 0, \tag{4.1}$$

and force equation,

$$m\left(\frac{\partial \mathbf{v}}{\partial t} + \mathbf{v}\cdot\nabla\mathbf{v}\right) + m\gamma\mathbf{v} = -\nabla\frac{\delta\mathscr{F}_{ex}[\hat{\rho}(\mathbf{r})]}{\delta\hat{\rho}}, \tag{4.2}$$

for the coarse-grained density $\rho(\mathbf{r},t)$ and the velocity field $\mathbf{v}(\mathbf{r},t)$, where γ is the drag coefficient and m is the mass of each particle. We will suppose that the excess free energy is given by the interaction potential energy plus a residual term, $\mathscr{F}_{ex}[\rho] = U[\rho] + \mathscr{F}_{res}[\rho]$, both functionals of coarse-grained density. Taking a time derivative of the second equation and using the first one, we obtain

$$m\left[\frac{\partial^2\mathbf{v}}{\partial t^2} + \frac{\partial(\mathbf{v}\cdot\nabla\mathbf{v})}{\partial t}\right] + m\gamma\frac{\partial\mathbf{v}}{\partial t} = \left[\frac{d\phi}{d\rho} + \frac{\rho}{2}\frac{d^2\phi}{d\rho^2} + \frac{d}{d\rho}\left(\frac{\delta\mathscr{F}_{res}[\rho]}{\delta\rho}\right)\right]\nabla[\nabla\cdot(\rho\mathbf{v})]. \tag{4.3}$$

By making a perturbation of the form $\rho(\mathbf{r},t) = \rho_0(\mathbf{r}) + \delta\rho_0 e^{i(\mathbf{k}\cdot\mathbf{r}-\omega t)}$ for the density and $\mathbf{v}(\mathbf{r},t) = \delta\mathbf{v}_0 e^{i(\mathbf{k}\cdot\mathbf{r}-\omega t)}$ for the velocity, linearizing and taking the limit $k\to 0$, we find $\omega(\omega + i\gamma) = c^2k^2$, where the sound speed c is given by

$$c^2 = \frac{\rho}{m}\left(\frac{d\phi(\rho)}{d\rho} + \frac{\rho}{2}\frac{d^2\phi(\rho)}{d\rho^2}\right) + \frac{\rho}{m}\frac{d}{d\rho}\left(\frac{\delta\mathscr{F}_{res}[\rho]}{\delta\rho}\right). \tag{4.4}$$

The same result can be obtained by a perturbation in the Dynamic Density Functional Theory (DDFT) equation for finite viscosity [73]

$$\frac{\partial^2\rho}{\partial t^2} + \gamma\frac{\partial\rho}{\partial t} = \frac{1}{m}\nabla\cdot\left[\rho\nabla\frac{\delta\mathscr{F}[\rho]}{\delta\rho}\right]. \tag{4.5}$$

On the other hand, the system of Newton's equations for all particles

$$m\frac{\partial^2 \mathbf{r}_i}{\partial t^2}+m\gamma\frac{\partial \mathbf{r}_i}{\partial t}=-\sum_{j\neq i}\nabla V_p(\mathbf{r}_{ij})=-\sum_{j\neq i}\hat{\mathbf{r}}_{ij}V_p'(r_{ij}), \tag{4.6}$$

where $\mathbf{r}_i$ is the position of particle i and $\hat{\mathbf{r}}_{ij}=(\mathbf{r}_i-\mathbf{r}_j)/|\mathbf{r}_i-\mathbf{r}_j|$, will give an exact result. By making a perturbation of the form $\mathbf{r}_i=\mathbf{r}_{0i}+\delta\mathbf{r}_i$ on the lattice positions and linearizing, we have

$$m\frac{\partial^2 \delta\mathbf{r}_i}{\partial t^2}+m\gamma\frac{\partial \delta\mathbf{r}_i}{\partial t}=-\sum_{j\neq i}\left\{[\delta\mathbf{r}_{ij}-\hat{\mathbf{r}}_{0ij}(\delta\mathbf{r}_{ij}\cdot\hat{\mathbf{r}}_{0ij})]\frac{V_p'(r_{0ij})}{r_{0ij}}+\hat{\mathbf{r}}_{0ij}(\delta\mathbf{r}_{ij}\cdot\hat{\mathbf{r}}_{0ij})V_p''(r_{0ij})\right\}. \tag{4.7}$$

Using $\delta\mathbf{r}_i(t)=\delta\mathbf{r}_0 e^{i(\mathbf{k}\cdot\mathbf{r}_{0i}-\omega t)}$,

$$m\omega(\omega+i\gamma)\delta\mathbf{r}_o=\sum_{j\neq i}(1-\cos(\mathbf{k}\cdot\mathbf{r}_{0ij}))\left\{\hat{\mathbf{r}}_{0ij}(\delta\mathbf{r}_{ij}\cdot\hat{\mathbf{r}}_{0ij})\left[V_p''(r_{0ij})-\frac{V_p'(r_{0ij})}{r_{0ij}}\right]+\delta\mathbf{r}_{ij}\frac{V_p'(r_{0ij})}{r_{0ij}}\right\}. \tag{4.8}$$

There are two types of waves satisfying $\omega(\omega+i\gamma)=c^2k^2$ for long wavelengths. They are the longitudinal ($\delta\mathbf{r}_0\parallel\mathbf{k}$) and transversal ($\delta\mathbf{r}_0\perp\mathbf{k}$) waves. After taking the limit $k\to 0$, the sound speed of longitudinal waves is independent of $\mathbf{r}_{0i}$ and given by the lattice sum [40]

$$c^2=\sum_i\frac{r_i^2\cos^2\theta_i}{2m}\left\{V_p''(r_i)\cos^2\theta_i+\frac{V_p'(r_i)}{r_i}\sin^2\theta_i\right\}. \tag{4.9}$$

In a triangular lattice, we can separate the sum in a collection of hexagons. For each term with angle θ_i in this sum, there are other five with same radius and angles $\theta_i+n\pi/3$ ($n=1,2,...,5$). Using the properties

$$\sum_{n=0}^{5}\cos^4\left(\theta_i+n\frac{\pi}{3}\right) = 6\langle\cos^4\theta\rangle=\frac{9}{4}, \tag{4.10}$$

$$\sum_{n=0}^{5}\cos^2\left(\theta_i+n\frac{\pi}{3}\right)\sin^2\left(\theta_i+n\frac{\pi}{3}\right) = 6\langle\cos^2\theta\sin^2\theta\rangle=\frac{3}{4}, \tag{4.11}$$

and then, using $r_i=\mathrm{x}p_i$, we finally obtain the sound speed

$$c^2 = \sum_i\frac{r_i}{16m}\left[V_p'(r_i)+3r_iV_p''(r_i)\right] \tag{4.12}$$

$$= \frac{\mathrm{x}}{16m}\left[\sum_i p_iV_p'(\mathrm{x}p_i)+3\mathrm{x}\sum_i p_i^2V_p''(\mathrm{x}p_i)\right] \tag{4.13}$$

$$= \frac{\mathrm{x}}{16m}\left[\frac{d}{d\mathrm{x}}\sum_i V_p(\mathrm{x}p_i)+3\mathrm{x}\frac{d^2}{d\mathrm{x}^2}\sum_i V_p(\mathrm{x}p_i)\right] \tag{4.14}$$

$$= \frac{\mathrm{x}}{16m}\left[\frac{d\phi(\mathrm{x})}{d\mathrm{x}}+3\mathrm{x}\frac{d^2\phi(\mathrm{x})}{d\mathrm{x}^2}\right] \tag{4.15}$$

$$= \frac{\rho}{m}\left[\frac{d\phi(\rho)}{d\rho}+\frac{3}{4}\rho\frac{d^2\phi(\rho)}{d\rho^2}\right], \tag{4.16}$$

where we used $r_i = \mathrm{x} p_i$ for each particle and the proportionality factor p_i depends on the lattice geometry.

Comparing equations (4.4) and (4.16) we can see that the dynamics of wave propagation needs an additional force given by

$$\mathbf{F}_{res} = -\frac{\rho}{4}\frac{d^2\phi(\rho)}{d\rho^2}\nabla\rho, \tag{4.17}$$

which can come from a residual free energy, given by

$$\mathscr{F}_{res}[\rho(\mathbf{r},t)] = -\frac{1}{2}\int \psi(\rho(\mathbf{r},t))d^2r, \tag{4.18}$$

where

$$\psi(\rho) = \int_0^\rho \phi(\rho')d\rho' - \frac{\rho\phi(\rho)}{2} + A\rho + B, \tag{4.19}$$

and A and B are constants of integration.

Notice that $-\mathscr{F}_{res}[\rho]$ has properties of entropy when $d^2\psi/d\rho^2 \leq 0$ by choosing A and B such that $\psi(0) = \psi(1) = 0$ [61]. Also, the convexity property,

$$\frac{d^2\psi(\rho)}{d\rho^2} = -\frac{\rho}{2}\frac{d^2\phi(\rho)}{d\rho^2} \leq 0, \tag{4.20}$$

is valid for many types of interaction such as power-law $V_p(r) \propto 1/r^m$, for $m > 2$ (which is also a necessary condition for convergency of equation (3.17)), and Yukawa $V_p(r) \propto e^{-\kappa r}/r$ interactions. The latter can be easily observed through the closed form approximations of $\phi(\rho)$ investigated in Section 1.3. Moreover, notice that, when the interaction range is much bigger than x and much smaller than the scale of density variations, one can use the approximation $\phi(\rho(\mathbf{r})) \approx \int \rho(\mathbf{r}')V_p(|\mathbf{r}-\mathbf{r}'|)d^2r' \approx \rho(\mathbf{r})\int V_p(\mathbf{r}')d^2r'$ and then the influence of $\mathscr{F}_{res}[\rho]$ is negligible.

For power law interactions $\phi(\rho) = C_m q^2/\mathrm{x}^m \propto \rho^{m/2}$, where C_m is a constant resulted from a lattice sum, $\mathscr{F}_{res}[\rho]$ can have the form of a Tsallis entropy [61],

$$\psi(\rho) = k\frac{[(\rho/A)^\nu - (\rho/A)]}{1-\nu}, \tag{4.21}$$

for appropriate choices of k and A, where the entropic-index ν is equal to $1+m/2$. J. S. Andrade Jr. et al. showed in [61] that the the negative of interaction potential energy (equation (3.16)) has the form of a Tsallis entropy with index $\nu = 2$. But, in fact, it is not a true entropy.

4.2 An equilibrium system

We recently performed computer simulations where a perfect crystal inside a retangular box (with periodic boundary conditions) is subject to an external force in the x-coordinate direction with potential of the type

$$V_{ext} = V_0 cos(2\pi x/L), \tag{4.22}$$

where V_0 is its amplitude, x is the position in one of the box directions and L is the box length in the x-direction. The interaction potential was a power law one, with power $m = 6$, i.e., $V_p(r) = q^2/r^6$. This potential is short-ranged and simple for computations. At small temperatures, the crystal, initially homogeneous (see Figure 4.1), evolves overdampedly towards an equilibrium inhomogeneous coarse-grained density (see Figure 4.2).

Figure 4.1 Initial state of our simulations, which is homogeneous. The particles are in a prefect triangular lattice configuration. Periodic boundary conditions are used.

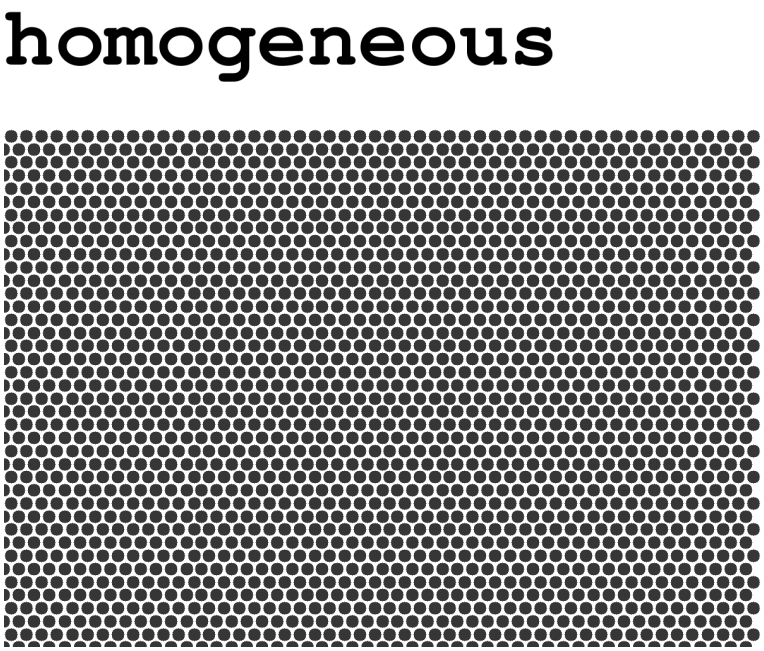

We simulated with many different number of particles up to 10^5 and found that, for small V_0 and consequently small density variations, the equilibrium configuration remains a triangular lattice without forming defects, but more elongated in some regions than in others. The force in this case relates to the density in the same way as in the case of sound waves. In fact, the density profile which minimizes the free energy $U_{ext}[\rho] + U_{int}[\rho] + \mathscr{F}_{res}[\rho]$ fits the simulation results much better than the one without $\mathscr{F}_{res}[\rho]$. The same results are found at zero and low finite temperatures.

These startling simulations exhibit a low temperature equilibrium system where the usual potential energy is not minimized. In fact, this is due to the initial configuration. On the other hand, initiating at the liquid state (high temperature) and then freezing and annealing till zero temperature, we obtain a configuration with defects, which tries to minimize the usual potential energy $U_{ext}[\rho] + U_{int}[\rho]$. The perfect crystal, at low temperatures, fails in forming defects when the external perturbation is sufficiently small.

Figure 4.2 Final state of our simulations, which is inhomogeneous. The particles are in a configuration of triangular lattice with distortions. Periodic boundary conditions are used.

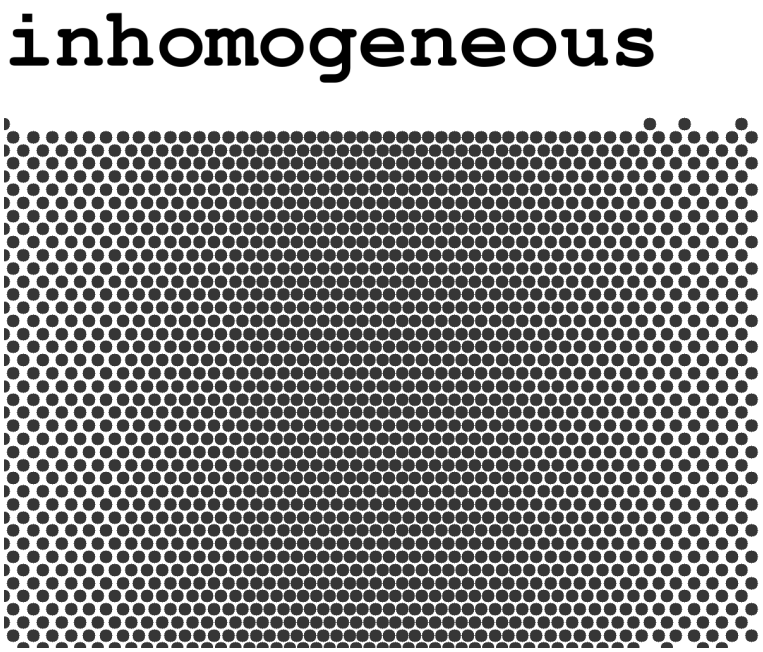

4.3 Summary of the Chapter

In this Chapter, we found that the equation for the force can be different, than that obtained in the previous one, in some systems where the inhomogeneity of coarse-grained density is produced without formation of any topological defects in the lattice. This is shown for long wavelenght longitudinal waves and an equilibrium system with a cosine type external potential. In these cases the force can be corrected by adding a residual term in the free energy.

CHAPTER 5

Conclusions

In this M.Sc. thesis, we investigated formulas for interaction forces and energy of two-dimensional crystals when inhomogeneity of coarse-grained density comes to play, at the zero temperature limit.

The interaction energy of a perfect crystal, with constant coarse-grained density, is given by a lattice sum and we called it Madelung energy. Some analytical approximations to it, investigated in a previous work, were showed. The relative error of a proposed method goes to zero in the continuum and nearest-neighbors asymptotic limits. The method is especially efficient in the case of Yukawa interactions, where closed forms and small relative errors are obtained.

In order to introduce a little bit about the importance and applicability of calculations of energy and forces in inhomogeneous systems, we presented a previous published work [42]. The density profile and the system's size of $2D$ complex plasma clusters confined by a parabolic potential are obtained analytically. For the calculation of the interaction energy, we used the Local Density Approximation with a position independent finite size effects. A differential equation for the density was obtained by a new method. Using the proposed interaction energy, this differential equation gives the same result of the variational and pressure approaches, however our method gives insight to a new important boundary condition. The boundary condition and the FSE were determinant to provide surprisingly good results in systems with relatively small number of particles ($8 < N < 500$). For instance, for $\alpha = 10^{-2}$, the relative error of the theoretical maximum radius of the system is less than 5% for any $N > 8$.

Then we look at the density functional way to obtain the interaction force due to a inhomogeneous density by means of DDFT. We presented a simple intuitive, but non-rigorous, derivation of this force. The microscopic approach developed for the complex plasma clusters is revisited and the same result of DDFT is obtained.

Thereafter, we investigated the calculation of the sound speed, the velocity of long wavelength longitudinal waves. The exact value of the sound speed can be obtained by perturbations in the system of Newton's equations for each particle. It turns out that the DDFT needs an additional term in the free energy in order to obey the correct value of the sound speed and use functionals of coarse-grained density.

Finally, recent simulations showed that the same correction term is needed when the crystal responds to a weak external potential, becoming inhomogeneous without forming any lattice defects. The defects would decrease the potential interaction energy. The additional term in the free energy will be subject of study in future works.

References

[1] A. Naumovets, A. Lyuksyutov, and V. Pokrovsky, *Two-Dimensional Crystals*. Elsevier Science, 2012. 1, 1.1

[2] W. Friedrich, P. Knipping, and M. Laue, "Interferenzerscheinungen bei rÃ¶ntgenstrahlen," *Annalen der Physik*, vol. 346, no. 10, pp. 971–988, 1913. 1

[3] R. Haüy, J.-B.-F. Gogue, Jean-Baptiste & Nee de La Rochelle, and A. G. Demonville, *Essai d'une theorie sur la structure des crystaux, appliquee a plusieurs genres de substances crystallisees; par M. l'abbe Hauy ..* chez Gogue & Nee de La Rochelle, libraires, quai des Augustins, pres le pont Saint-Michel, 1784. 1

[4] A. Schoenflies, *Kristallsysteme und Kristallstruktur*. Druck und verlag von BG Teubner, 1891. 1

[5] E. Fedorov, "Simmetrija na ploskosti (symmetrie in der ebene)," *Zapiski Imperatorskogo Sant-Petersburgskogo Mineralogicheskogo Obshchestva*, vol. 28, no. 245-291, 1891. 1

[6] R. Masel, *Principles of Adsorption and Reaction on Solid Surfaces*. A Wiley-Interscience publication, Wiley, 1996. 1.1

[7] J. Hudson, *Surface Science: An introduction*. Elsevier Science, 2013. 1.1

[8] A. A. Abrikosov, "On the Magnetic properties of superconductors of the second group," *Sov. Phys. JETP*, vol. 5, pp. 1174–1182, 1957. [Zh. Eksp. Teor. Fiz.32,1442(1957)]. 1.1

[9] J. Hu and A. H. MacDonald, "Two-dimensional vortex lattice melting," *Phys. Rev. Lett.*, vol. 71, pp. 432–435, Jul 1993. 1.1

[10] C. C. Grimes and G. Adams, "Evidence for a liquid-to-crystal phase transition in a classical, two-dimensional sheet of electrons," *Phys. Rev. Lett.*, vol. 42, pp. 795–798, Mar 1979. 1.1

[11] A. H. C. Neto and K. Novoselov, "New directions in science and technology: two-dimensional crystals," *Reports on Progress in Physics*, vol. 74, no. 8, p. 082501, 2011. 1.1

[12] W. F. Brinkman, D. S. Fisher, and D. E. Moncton, "Melting of two-dimensional solids," *Science*, vol. 217, no. 4561, pp. 693–700, 1982. 1.1

[13] X. H. Zheng and R. Grieve, "Melting behavior of single two-dimensional crystal," *Phys. Rev. B*, vol. 73, p. 064205, Feb 2006. 1.1, 1.2

[14] M. Saint Jean, C. Guthmann, and G. Coupier, "Relaxation and ordering processes in "macroscopic wigner crystals"," *The European Physical Journal B - Condensed Matter and Complex Systems*, vol. 39, no. 1, pp. 61–68, 2004. 1.1

[15] P. Pierański, *Gravity's Rainbow - Structure of a 2D Crystal Grown in a Strong Gravitational Field*, pp. 45–48. Boston, MA: Springer US, 1989. 1.3, 1.1

[16] G. A. Hebner, M. E. Riley, D. S. Johnson, P. Ho, and R. J. Buss, "Direct determination of particle-particle interactions in a 2d plasma dust crystal," *Phys. Rev. Lett.*, vol. 87, p. 235001, Nov 2001. 1.4, 1.1, 1.3.2

[17] L. Landau, "Zur theorie der energieubertragung. ii," *Physics of the Soviet Union*, vol. 2, no. 2, pp. 46–51, 1932. 1.2

[18] R. Peierls, "Quelques propriétés typiques des corps solides," *Annales de l'institut Henri Poincaré*, vol. 5, no. 3, pp. 177–222, 1935. 1.2

[19] H.-H. von Grünberg, P. Keim, and G. Maret, *Phase Transitions in Two-Dimensional Colloidal Systems*, pp. 41–86. Wiley-VCH Verlag GmbH & Co. KGaA, 2007. 1.5, 1.2

[20] L. Onsager, "Crystal statistics. i. a two-dimensional model with an order-disorder transition," *Phys. Rev.*, vol. 65, pp. 117–149, Feb 1944. 1.2

[21] B. J. Alder and T. E. Wainwright, "Phase transition in elastic disks," *Phys. Rev.*, vol. 127, pp. 359–361, Jul 1962. 1.2

[22] N. D. Mermin and H. Wagner, "Absence of ferromagnetism or antiferromagnetism in one- or two-dimensional isotropic heisenberg models," *Phys. Rev. Lett.*, vol. 17, pp. 1133–1136, Nov 1966. 1.2

[23] B. Jancovici, "Infinite susceptibility without long-range order: The two-dimensional harmonic "solid"," *Phys. Rev. Lett.*, vol. 19, pp. 20–22, Jul 1967. 1.2

[24] P. C. Hohenberg, "Existence of long-range order in one and two dimensions," *Phys. Rev.*, vol. 158, pp. 383–386, Jun 1967. 1.2

[25] N. D. Mermin, "Crystalline order in two dimensions," *Phys. Rev.*, vol. 176, pp. 250–254, Dec 1968. 1.2

[26] V. L. Berezinskiĭ, "Destruction of Long-range Order in One-dimensional and Two-dimensional Systems having a Continuous Symmetry Group I. Classical Systems," *Soviet Journal of Experimental and Theoretical Physics*, vol. 32, p. 493, 1971. 1.2

[27] J. Fröhlich and C. Pfister, "On the absence of spontaneous symmetry breaking and of crystalline ordering in two-dimensional systems," *Communications in Mathematical Physics*, vol. 81, no. 2, pp. 277–298, 1981. 1.2

[28] J. Fröhlich and C.-E. Pfister, "Absence of crystalline ordering in two dimensions," *Communications in Mathematical Physics*, vol. 104, no. 4, pp. 697–700, 1986. 1.2

[29] H. otto Georgii, "Translation invariance and continuous symmetries in two-dimensional continuum systems," in *Mathematical results in Statistical Mechanics, Singapore etc., World Scientific*, pp. 53–69, 1999. 1.2

[30] D. Ioffe, S. Shlosman, and Y. Velenik, "2d models of statistical physics with continuous symmetry: The case of singular interactions," *Communications in Mathematical Physics*, vol. 226, no. 2, pp. 433–454, 2002. 1.2

[31] H. E. Stanley and T. A. Kaplan, "Possibility of a phase transition for the two-dimensional heisenberg model," *Phys. Rev. Lett.*, vol. 17, pp. 913–915, Oct 1966. 1.2

[32] J. M. Kosterlitz and D. J. Thouless, "Ordering, metastability and phase transitions in two-dimensional systems," *Journal of Physics C: Solid State Physics*, vol. 6, no. 7, p. 1181, 1973. 1.2

[33] B. I. Halperin and D. R. Nelson, "Theory of two-dimensional melting," *Phys. Rev. Lett.*, vol. 41, pp. 121–124, Jul 1978. 1.2

[34] D. R. Nelson and B. I. Halperin, "Dislocation-mediated melting in two dimensions," *Phys. Rev. B*, vol. 19, pp. 2457–2484, Mar 1979. 1.2

[35] A. P. Young, "Melting and the vector coulomb gas in two dimensions," *Phys. Rev. B*, vol. 19, pp. 1855–1866, Feb 1979. 1.2

[36] F. Merkl and S. Rolles, "Spontaneous breaking of continuous rotational symmetry in two dimensions," *Electron. J. Probab.*, vol. 14, pp. 1705–1726, 2009. 1.2

[37] P. C. Martin, O. Parodi, and P. S. Pershan, "Unified hydrodynamic theory for crystals, liquid crystals, and normal fluids," *Phys. Rev. A*, vol. 6, pp. 2401–2420, Dec 1972. 1.2

[38] A. Zippelius, B. I. Halperin, and D. R. Nelson, "Dynamics of two-dimensional melting," *Phys. Rev. B*, vol. 22, pp. 2514–2541, Sep 1980. 1.2

[39] L.-J. Hou, Y.-N. Wang, and Z. L. Mišković, "Theoretical study of laser-excited mach cones in dusty plasmas," *Phys. Rev. E*, vol. 70, p. 056406, Nov 2004. 1.2, 4.1

[40] D. H. E. Dubin, "The phonon wake behind a charge moving relative to a two-dimensional plasma crystal," *Physics of Plasmas*, vol. 7, no. 10, pp. 3895–3903, 2000. 1.2, 4.1

[41] H. Totsuji, C. Totsuji, and K. Tsuruta, "Structure of finite two-dimensional yukawa lattices: Dust crystals," *Phys. Rev. E*, vol. 64, p. 066402, Nov 2001. 1.2, 2.1, 2.3.1, 2.3.2, 2.3.3, 2.4, 2.4, 2.5, 2.3

[42] P. C. N. Pereira, F. C. O. Silva, and S. W. S. Apolinario, "Continuum theory for two-dimensional complex plasma clusters," *New Journal of Physics*, vol. 15, no. 9, p. 093004, 2013. 1.2, 1.4, 2, 5

[43] P. Ehrenfest and T. Ehrenfest, *The Conceptual Foundations of the Statistical Approach in Mechanics*. Dover Books on Physics, Dover Publications, 2014. 1.2

[44] A. N. Gorban, *Basic Types of Coarse-Graining*, pp. 117–176. Berlin, Heidelberg: Springer Berlin Heidelberg, 2006. 1.2

[45] P. C. N. Pereira and S. W. S. Apolinario, "Madelung energy of yukawa lattices," *Phys. Rev. E*, vol. 86, p. 046702, Oct 2012. 1.3.2, 1.6, 1.4, 1.7, 2.3.1

[46] S. Auer and D. Frenkel, "Crystallization of weakly charged colloidal spheres: a numerical study," *Journal of Physics: Condensed Matter*, vol. 14, no. 33, p. 7667, 2002. 1.3.2

[47] M. Bonitz, C. Henning, and D. Block, "Complex plasmas: a laboratory for strong correlations," *Reports on Progress in Physics*, vol. 73, no. 6, p. 066501, 2010. 1.3.2, 2.1

[48] G. A. Hebner, M. E. Riley, and K. E. Greenberg, "Analysis of the particle interactions in a two-dimensional-plasma dust crystal and the use of dust as a probe of the time-averaged presheath electric field," *Phys. Rev. E*, vol. 66, p. 046407, Oct 2002. 1.3.2, 2.1, 2.3.1, 2.3.2, 2.4, 2.4, 2.5, 2.3

[49] A. Melzer, M. Klindworth, and A. Piel, "Normal modes of 2d finite clusters in complex plasmas," *Phys. Rev. Lett.*, vol. 87, p. 115002, Aug 2001. 2.1

[50] S. K. Zhdanov, M. H. Thoma, and G. E. Morfill, "Spontaneous disordering of a two-dimensional (2d) plasma crystal," *New Journal of Physics*, vol. 13, no. 1, p. 013039, 2011. 2.1

[51] C. Killer, A. Schella, T. Miksch, and A. Melzer, "Vertically elongated three-dimensional yukawa clusters in dusty plasmas," *Phys. Rev. B*, vol. 84, p. 054104, Aug 2011. 2.1

[52] S. Zhdanov, R. A. Quinn, D. Samsonov, and G. E. Morfill, "Large-scale steady-state structure of a 2d plasma crystal," *New Journal of Physics*, vol. 5, no. 1, p. 74, 2003. 2.1

[53] S. W. S. Apolinario, B. Partoens, and F. M. Peeters, "Structural and dynamical aspects of small three-dimensional spherical coulomb clusters," *New Journal of Physics*, vol. 9, no. 8, p. 283, 2007. 2.1

[54] H. Baumgartner, D. Asmus, V. Golubnychiy, P. Ludwig, H. Kählert, and M. Bonitz, "Ground states of finite spherical yukawa crystals," *New Journal of Physics*, vol. 10, no. 9, p. 093019, 2008. 2.1

[55] C. Henning, H. Baumgartner, A. Piel, P. Ludwig, V. Golubnichiy, M. Bonitz, and D. Block, "Ground state of a confined yukawa plasma," *Phys. Rev. E*, vol. 74, p. 056403, Nov 2006. 2.1

[56] C. Henning, P. Ludwig, A. Filinov, A. Piel, and M. Bonitz, "Ground state of a confined yukawa plasma including correlation effects," *Phys. Rev. E*, vol. 76, p. 036404, Sep 2007. 2.1, 2.3.1

[57] H. Totsuji, T. Ogawa, C. Totsuji, and K. Tsuruta, "Structure of spherical yukawa clusters: A model for dust particles in dusty plasmas in an isotropic environment," *Phys. Rev. E*, vol. 72, p. 036406, Sep 2005. 2.1

[58] T. Ott, M. Stanley, and M. Bonitz, "Non-invasive determination of the parameters of strongly coupled 2d yukawa liquids," *Physics of Plasmas*, vol. 18, no. 6, 2011. 2.1

[59] Z. L. Ye and E. Zaremba, "Magnetoplasma excitations in anharmonic electron dots," *Phys. Rev. B*, vol. 50, pp. 17217–17229, Dec 1994. 2.1

[60] M. Golosovsky, Y. Saado, and D. Davidov, "Energy and symmetry of self-assembled two-dimensional dipole clusters in magnetic confinement," *Phys. Rev. E*, vol. 65, p. 061405, Jun 2002. 2.1

[61] J. S. Andrade, G. F. T. da Silva, A. A. Moreira, F. D. Nobre, and E. M. F. Curado, "Thermostatistics of overdamped motion of interacting particles," *Phys. Rev. Lett.*, vol. 105, p. 260601, Dec 2010. 2.1, 2.3.4, 4.1, 4.1, 4.1

[62] J. S. A. Jr., G. F. T. da Silva, A. A. Moreira, F. D. Nobre, and E. M. F. Curado, "Surrejoinder to the comment on: "thermostatistics of overdamped motion of interacting particles" by y. levin and r. pakter," 2011. 2.3.4

[63] C. Totsuji, M. S. Liman, K. Tsuruta, and H. Totsuji, "Estimation of screening length and electric charge on particles in single-layered dusty plasma crystals," *Phys. Rev. E*, vol. 68, p. 017401, Jul 2003. 2.3.4

[64] M. Kong, B. Partoens, and F. M. Peeters, "Structural, dynamical and melting properties of two-dimensional clusters of complex plasmas," *New Journal of Physics*, vol. 5, no. 1, p. 23, 2003. 2.4

[65] R. Evans, "The nature of the liquid-vapour interface and other topics in the statistical mechanics of non-uniform, classical fluids," *Advances in Physics*, vol. 28, no. 2, pp. 143–200, 1979. 3

[66] U. M. B. Marconi and P. Tarazona, "Dynamic density functional theory of fluids," *Journal of Physics: Condensed Matter*, vol. 12, no. 8A, p. A413, 2000. 3

[67] B. D. Goddard, A. Nold, N. Savva, G. A. Pavliotis, and S. Kalliadasis, "General dynamical density functional theory for classical fluids," *Phys. Rev. Lett.*, vol. 109, p. 120603, Sep 2012. 3

[68] J. Reinhardt and J. M. Brader, "Dynamics of localized particles from density functional theory," *Phys. Rev. E*, vol. 85, p. 011404, Jan 2012. 3, 3.1, 3.1

[69] M. Rex and H. Löwen, "Dynamical density functional theory with hydrodynamic interactions and colloids in unstable traps," *Phys. Rev. Lett.*, vol. 101, p. 148302, Sep 2008. 3

[70] A. Fortini, D. de las Heras, J. M. Brader, and M. Schmidt, "Superadiabatic forces in brownian many-body dynamics," *Phys. Rev. Lett.*, vol. 113, p. 167801, Oct 2014. 3

[71] J. F. Lutsko, *Recent Developments in Classical Density Functional Theory*, pp. 1–92. John Wiley & Sons, Inc., 2010. 3.1

[72] A. Mughal and M. A. Moore, "Topological defects in the crystalline state of one-component plasmas of nonuniform density," *Phys. Rev. E*, vol. 76, p. 011606, Jul 2007. 3.3

[73] A. J. Archer, "Dynamical density functional theory for molecular and colloidal fluids: A microscopic approach to fluid mechanics," *The Journal of Chemical Physics*, vol. 130, no. 1, 2009. 4.1